

UKAEA-CCFE-PR(20)23

F. Koechl, R. Ambrosino, P. Belo, M. Cavinato, G. Corrigan, L. Garzotti, D. Harting, A. Kukushkin, A. Loarte, M. Mattei, E. Militello-Asp, V. Parail, M. Romanelli, G. Saibene, R. Sartori

# **Evaluation of fuelling requirements for core density and divertor heat load control in non-stationary phases of the ITER DT 15 MA baseline scenario**

Enquiries about copyright and reproduction should in the first instance be addressed to the UKAEA Publications Officer, Culham Science Centre, Building K1/O/83 Abingdon, Oxfordshire, OX14 3DB, UK. The United Kingdom Atomic Energy Authority is the copyright holder.

The contents of this document and all other UKAEA Preprints, Reports and Conference Papers are available to view online free at [scientific-publications.ukaea.uk/](https://scientific-publications.ukaea.uk/)

# **Evaluation of fuelling requirements for core density and divertor heat load control in non-stationary phases of the ITER DT 15 MA baseline scenario**

F. Koechl, R. Ambrosino, P. Belo, M. Cavinato, G. Corrigan, L. Garzotti, D. Harting, A. Kukushkin, A. Loarte, M. Mattei, E. Militello-Asp, V. Parail, M. Romanelli, G. Saibene, R. Sartori



## Evaluation of fuelling requirements for core density and divertor heat load control in non-stationary phases of the ITER DT 15 MA baseline scenario

F. Koechl<sup>1,2</sup>, R. Ambrosino<sup>3</sup>, P. Belo<sup>1</sup>, M. Cavinato<sup>4</sup>, G. Corrigan<sup>1</sup>, L. Garzotti<sup>1</sup>,  
D. Harting<sup>1</sup>, A. Kukushkin<sup>5,a</sup>, A. Loarte<sup>5</sup>, M. Mattei<sup>3</sup>, E. Militello-Asp<sup>1</sup>,  
V. Parail<sup>1</sup>, M. Romanelli<sup>1</sup>, G. Saibene<sup>4</sup> and R. Sartori<sup>4</sup>

<sup>1</sup>*Culham Centre for Fusion Energy, Culham Science Centre, Abingdon, OX14 3DB, UK*

<sup>2</sup>*Fusion@ÖAW, Atominstitut, TU Wien, Stadionallee 2, 1020 Vienna, Austria*

<sup>3</sup>*CREATE, University of Naples 'Federico II', Italy*

<sup>4</sup>*Fusion For Energy Joint Undertaking, Josep Pla 2, 08019 Barcelona, Spain*

<sup>5</sup>*ITER Organization, Route de Vinon-sur-Verdon, CS 90 046,  
13067 St Paul Lez Durance Cedex, France.*

E-mail: [Florian.Koechl@ukaea.uk](mailto:Florian.Koechl@ukaea.uk)

**Abstract.** To ensure optimal plasma performance at high  $Q_{\text{fus}}$  for the baseline scenario foreseen for the International Tokamak Experimental Reactor (ITER), the fuelling requirements, in particular for non-stationary phases, need to be assessed by means of integrated modelling to address the special additional challenges facing plasma fuelling on ITER. The fuelling scheme needs to be adjusted to ensure robust divertor heat load control, avoiding complete detachment while still maintaining low divertor temperatures and heat fluxes to minimise W sputtering and erosion of the plasma facing components (PFCs). At the same time, the core density needs to be controlled to fulfil requirements for: the application of neutral beam heating; a robust transition from L-mode to stationary fusion burn; the maximisation of the fusion yield; and a fast reduction in core particle content in the termination phase.

Coupled core-edge-SOL transport calculations have been performed, simulating for the first time the entire ITER plasma evolution from just after the X-point formation until the late termination phase. These calculations are being exploited to find the most effective ways of fuelling and heating DT plasmas without exceeding ITER operational limits (e.g. divertor power density). The most efficient ways to fuel ITER with gas and / or pellet injection have been investigated self-consistently with the integrated core+edge+SOL transport suite of codes, JINTRAC, developed at JET [Romanelli PFR 2014].

Our modelling is exploited to propose schemes for gas and pellet fuelling for main ion SOL and core density control, respectively, and for impurity seeding by Ne for the control of SOL radiation, that allow ITER to approach  $Q_{\text{fus}} \sim 10$ , with plasma evolution successfully controlled to respect major operational limits through all transients from the early ramp-up until the late ramp down phase.

### 1. Introduction

Good insights on optimising performance will be essential for helping ITER reach its primary goal of achieving high  $Q_{\text{fus}}$  (cf. e.g. [Parail NF 2013, Kessel NF 2015, Kim NF 2018]). In present devices the edge plasma is fairly transparent to gas fuelling, which implies efficient core fuelling even without pellet injection. In contrast, ITER will feature a hot and dense edge plasma and recycled gas and most fuel gas will be ionised in the far scrape-off-layer (SOL) and not reach the separatrix [Kukushkin PPCF 2002, Romanelli NF 2015]. Thus, pellet injection, albeit peripheral, will be vital to fuel the ITER core plasma. The density evolution will be key to determining the heating scheme to reach  $Q_{\text{fus}} = 10$  H-mode. Here, for the first time, coupled core+edge+SOL transport modelling calculations have been carried out for the ITER 15 MA / 5.3 T DT baseline scenario that follow the entire plasma evolution from just after X-point formation until the late current ramp-down phase to find the most effective ways of fuelling and heating DT plasmas without exceeding ITER operational limits: e.g. minimising neutral beam (NB) shine-through, and limiting divertor power fluxes to

---

<sup>a</sup> Present addresses:

NRC Kurchatov Institute, Kurchatov sq. 1, 123182 Moscow, Russian Federation  
NRNU MEPhI, Kashirskoye av. 31, 115409 Moscow, Russian Federation

$< 10 \text{ MW/m}^2$ . The most efficient ways to fuel ITER with gas and/or pellet injection have been investigated self-consistently with the integrated core+edge+SOL transport suite of codes, JINTRAC, developed at JET [Romanelli PFR 2014], which combines: JETTO/SANCO, a 1.5D core transport solver including impurities [Cenacchi JET-IR 1988, Lauro-Taroni EPS 1994]; and EDGE2D/EIRENE, a 2D SOL/edge multi-fluid solver, combined with a kinetic Monte Carlo neutral transport code, that includes plasma interactions with the ITER Be wall and W divertor [Simonini CPP 1994, Reiter JNM 1992]. This study has been performed as part of a broader modelling activity carried out within the framework of an ITER Task Agreement (C19TD51FE) implemented by Fusion for Energy under Grant GRT-502 as summarised in [Militello-Asp NF 2019].

At a given input power, as the gas rate is increased in the simulations, the core density increases and then saturates [Romanelli NF 2015]. If attempts are made to increase the gas rate beyond saturation, the density builds up in the SOL, due to poor neutral penetration and insufficient power fluxes, and this may lead to completely detached unstable divertor conditions and possibly a MARFE (multifaceted asymmetric radiation from the edge) [Lipschultz NF 1984]. It has recently been demonstrated in the experiment, that stable strongly detached regimes can be realised under certain conditions, albeit at reduced edge confinement [Kallenbach NF 2015]. Although they could in principle also be foreseen for ITER divertor operation, this option is not considered in the simulations as a conservative approach. There are indications from previous JINTRAC studies that the maximum Greenwald density fraction  $n_{e,\text{lin.avg.}}/n_{\text{GW}}$  that can be achieved with gas fuelling alone in the current ramp-up phase of the ITER DT baseline L-mode phase may be limited to  $< \sim 30\%$ , depending on the applied heating power (cf. [Belo EPS 2015, Garzotti EPS 2016]). Routine use of pellets might then be required in order to reach sufficient density for absorption of NB power with acceptably low shine-through losses. In this paper, JINTRAC simulations are used to explore the range of  $n_{e,\text{lin.avg.}}/n_{\text{GW}}$  that can be sustained while respecting all constraints for divertor operation during the current ramp-up phase as function of the applied power and current ramp rate.

In the 15MA / 5.3T DT baseline plasma, the heat flux at the separatrix  $P_{\text{sep}}$  might only slightly exceed the L-H transition threshold and alpha heating might be essential to reach a good quality ELMy H-mode [Loarte NF 2014]. The density ramp-up after the L-H transition might require careful tuning of the particle throughput from gas and pellets to avoid overloading the divertor and inducing full detachment, while providing enough fuelling to reach the density required for  $Q_{\text{fus}} \sim 10$ . With the integrated modelling approach presented here, the viability of a heating (33 MW NB + 20 MW ECRH) and fuelling scheme to reach  $Q_{\text{fus}} \sim 10$  is investigated, comparing plasma scenarios where the L-H transition occurs during and after the end of the plasma current ramp (at  $I_{\text{pl}} = 10 \text{ MA}$ , and  $I_{\text{pl}} = 15 \text{ MA}$ , respectively). The question is addressed whether the foreseen divertor control schemes are compatible with given constraints on core fuelling in the transition to a burning plasma at high  $Q_{\text{fus}}$  [Loarte NF 2013, Koechl NF 2017]. In particular, we assess whether the level of SOL radiation needed to protect the divertor can be established quickly enough by impurity seeding when the (time-averaged) heat flux to the divertor is strongly increased at the start of the ELMy H-mode phase that is associated with a reduction in the increase in thermal energy content,  $dW_{\text{th}}/dt$ .

For the establishment of the ITER baseline scenario, challenges need to be met not only on the path from early ramp-up to stationary burning plasma conditions, but also for the controlled termination of the discharge, considering the back transition to low confinement and the reduction in plasma current [Loarte NF 2014, de Vries NF 2017, Poli FEC 2018]. Scenarios have been developed, using JINTRAC simulations, to handle the H-L transition and current ramp-down while simultaneously satisfying all operational constraints to protect the divertor and keep the divertor plasma stable. Starting from quasi-stationary pellet-fuelled high

density H-mode flat-top conditions at  $Q_{\text{fus}} \sim 10$  as described in [Garzotti NF 2019, Militello-Asp NF 2019], the plasma current ramp-down phase is modelled with the H-L transition occurring at the maximum current ( $I_{\text{pl}} = 15$  MA), and part way through the current ramp down (at  $I_{\text{pl}} = 10$  MA). Once again, special emphasis is placed on assessing impurity seeding feedback control that must provide a strongly time dependent target level of divertor radiation during transients encountered in the ramp-down phase. In addition, pump requirements to keep the density below the Greenwald limit throughout the current ramp-down phase are assessed.

Section 2 provides a short description of simulation settings and model assumptions. This is followed by a detailed description of the core+edge+SOL modelling results and an assessment of fuelling requirements for core density and divertor control for the complete plasma evolution in the 15MA / 5.3T ITER DT baseline scenario including non-stationary phases. The transition from the early diverted current ramp-up phase to a burning high  $Q_{\text{fus}}$  regime is described in Section 3. Section 4 gives modelling results for the latter part of the discharge, covering the transition from the stationary high  $Q_{\text{fus}}$  phase through the H-L transition and  $I_{\text{pl}}$  ramp down. A short summary is provided in Section 5.

## 2. Simulation setup

The modelling of the ITER DT 15 MA / 5.3 T baseline in this paper uses similar tools and transport modelling assumptions that have been used in other recent work [Romanelli NF 2015, Belo EPS 2015, Garzotti EPS 2016, Militello-Asp NF 2019, Garzotti NF 2019]. They have recently been validated against non-stationary ITER-relevant JET plasma conditions [Koechl NF 2017, Koechl PPCF 2018].

All JINTRAC simulations discussed in this paper have been carried out modelling the plasma evolution in the core, edge and SOL region including the interaction with PFCs, by combination of the core transport code JETTO+SANCO with the SOL transport code EDGE2D+EIRENE [Fichtmüller CJP 1998]. Transport in the core and edge region is described by solution of transport equations for  $q$ ,  $p_e$ ,  $p_i$ ,  $n_D$ ,  $n_T$  and a selection of up to two impurity species ( $n_{\text{He}}$ ,  $n_{\text{Be}}$ , or  $n_{\text{Ne}}$ , depending on the scenario phase in consideration). W transport has not been taken into account.<sup>a</sup>

Neoclassical transport in the core and edge is modelled by NCLASS [Houlberg PoP 1997] for main ions and all impurity stages except for Ne, which is described by application of a bundling scheme with five super-stages in SANCO [Summers AIP 2007]. Anomalous transport is described by the Bohm/gyro-Bohm (BgB) H-mode model [Erba PPCF 1997] together with a collisionality dependent inwards pinch term. Coefficients were adapted in order to match ITER predictions obtained with the gyro-Landau fluid model GLF-23 [Waltz PoP 1997] as described in [Garzotti NF 2012, Romanelli NF 2015] in the H-mode phases of the discharge, and by the standard Bohm/gyroBohm L-mode model [Erba JET-R 1996, Bizarro PPCF 2016] (including an inwards pinch term proportional to  $0.5 \cdot D_{i,\text{BgB}}$ ) when the plasma is in L-mode. Impurity reaction cross-sections are evaluated by ADAS [Summers ADAS 2001]. As  $P_{\text{net}} := P_{\text{in}} - dW_{\text{th}}/dt$  approaches  $P_{\text{L-H}}$  from above, the transport in the ETB is gradually increased by applying a (reducing) suppression factor  $\exp(- (P_{\text{net}} - P_{\text{L-H}}) / (\lambda \cdot P_{\text{L-H}}))$  to the anomalous heat and particle diffusivities within the ETB,  $\chi_{e/i,\text{ETB}}$ , and  $D_{i/\text{imp},\text{ETB}}$  (cf. [Loarte NF 2014]). The parameter  $\lambda$  is chosen such that anomalous transport is almost fully suppressed for  $P_{\text{net}}/P_{\text{L-H}} > \sim 1.3-1.5$  while it remains significant for lower  $P_{\text{net}}/P_{\text{L-H}}$  mimicking

---

<sup>a</sup> The implicit assumption is thus made that the PFCs are always sufficiently well protected to keep W sputtering rates sufficiently low such that the plasma contamination by W and its impact on plasma conditions remain negligible.

the effect of reduced H-mode confinement in that case in accordance with experimental observations [Sartori PPCF 2004].  $P_{L-H}$  is prescribed in the simulations by the scaling proposed in [Martin JoP 2008]. Resistivity and bootstrap current density are calculated by NCLASS. Momentum transport is determined by the momentum source due to NB injection and assuming a Prandtl number equal to one to prescribe the momentum diffusivity.

The effect of sawteeth on the current density and kinetic profiles is described in a time-averaged way by applying the “Continuous Sawtooth model”. With this model, the time-averaged profile flattening in the core region that would be obtained by applying a discrete sawtooth model is emulated by applying the value of the neoclassical resistivity evaluated at  $q \sim 1.0$  in the sawtooth-affected region where  $q < 1.0$  and by an increase of the heat and particle diffusivities  $\chi_{e/i}$  and  $D_{i/imp}$  by  $\sim 0.3-0.5 \text{ m}^2/\text{s}$  in that zone. The effect of ELMs is also considered in a time-averaged way using the Continuous ELM model described in [Parail NF 2009]. The pedestal width and the maximum achievable pedestal pressure due to MHD constraints are imposed to be in agreement with EPED1 scaling predictions [Snyder PoP 2009, Polevoi NF 2015].

Auxiliary heating by neutral beams is either modelled with PENCIL [Challis NF 1989] or ASCOT [Heikkinen PoP 1995, Hirvijoki CPC 2014], while ECRH heat and current sources are determined by a scaling approximation based on GRAY calculations [Farina FSciTec 2007].

The plasma is mainly fuelled in the simulations by neutral atoms due to gas puffing and recycling (applying a wall recycling coefficient of 1.0 for D) and by pellets with particle deposition profiles being modelled by HPI2 [Pégourié NF 2005, Pégourié NF 2007].

The magnetic equilibrium is recalculated every  $\sim 100$  ms with the 2D equilibrium solver ESCO (including the pressure contribution from fast particles). A fixed full bore plasma shape is prescribed that has been derived from free boundary calculations with the CREATE-NL code [Albanese NF 2004]. This has been confirmed to be achievable and sustainable for all plasma current levels and current ramp rates considered in the modelling ( $I_{pl} > 3$  MA), provided that (i) the internal plasma inductance remains within the limits for efficient plasma shape and vertical stability control, and (ii) limits in poloidal flux consumption are respected. (For a detailed analysis of plasma shape and stability control with CREATE-NL for the ITER DT 15 MA / 5.3 T baseline scenario, see e.g. [Parail NF 2013, Mattei FED 2009].).

Standard ITER wall and pump structures and assumptions are applied as described in [Romanelli NF 2015]. Parallel heat and particle transport in the SOL is determined by the standard Braginskij model [Braginski RevPP 1965], and perpendicular transport is prescribed using radially dependent diffusion coefficients and convection velocities as described in [Wiesen PPCF 2011]. In the near-SOL, the prescribed transport coefficients are set to match the coefficients set by the core-edge transport models at the separatrix. Further away from the separatrix (at  $R-R_{sep} > \sim 0 / 0.5$  cm in the outer mid-plane in L-mode / H-mode resp.) the transport coefficients are set to gradually approach prescribed far-SOL values of  $\chi_e = \chi_i = 1.0 \text{ m}^2/\text{s}$ ,  $D_{D/T} = D_{imp} = 0.3 \text{ m}^2/\text{s}$  (cf. [Kukushkin JNM 2013]). For a sensitivity scan in SOL transport coefficient assumptions, see [Romanelli NF 2015, Belo EPS 2015]). Cross-field drifts in the SOL are not included in the simulations.

The maximum time step used for the integration of the transport equations in EDGE2D is set to  $\sim 1-5 \mu\text{s}$ . To reduce the required computation time for these CPU-intensive simulations, a partial coupling scheme is applied (cf. [Fichtmüller CJP 1998]) with user prescribed time intervals of  $\Delta t_1 = 15-20$  ms and  $\Delta t_2 = 1$  ms for phases when JETTO+SANCO is evolved alone with fixed boundary conditions, and phases when JETTO+SANCO and EDGE2D+EIRENE are coupled and boundary conditions are exchanged at each time step, respectively. A partial coupling correction scheme is applied, in which correction particle source terms are

introduced in EDGE2D+EIRENE in the coupled phase to minimise the error in the time-averaged evolution of SOL particle content with respect to an exact fully coupled calculation. The correction terms are estimated from the time history of the SOL particle content. As this error grows with the duration of the non-coupled phase,  $\Delta t_1$  is automatically reduced by the correction scheme if the correction particle source terms become sizeable. For the description of neutral dynamics,  $\sim 10000$  Monte Carlo particles have been used in each EIRENE iteration which is carried out every  $\sim 1-30$  EDGE2D time steps. EIRENE is run in time-independent mode, assuming that neutral transport is quasi-stationary, which is a reasonable assumption, as the transport time scales of transients in the simulations presented here always exceed the time scale for neutral transport equilibration. Regarding other edge modelling assumptions, the standard EDGE2D+EIRENE plasma-wall interaction models are used.

### 3. Transition from early current ramp-up phase to burning high $Q_{\text{fus}}$ regime

#### 3.1 Current ramp-up

In these simulations, a scenario with early transition from the limiter to divertor configuration is considered, where the plasma is in a diverted configuration for  $t > 10$  s,  $I_p > 3$  MA. The plasma is fuelled by application of DT gas puff only. Auxiliary heating is provided by ECRH only in this phase, with a maximum applied power of 20 MW. The peak in EC power deposition is located at  $\rho_{\text{norm}}=0.2$ .

##### 3.1.1 Scan in applied nominal DT gas puff rates

In this scan, the plasma current  $I_{\text{pl}}$  is linearly ramped up from 3 MA to 15 MA for  $t = 10-80$  s. During this period, a constant nominal DT gas puff rate is applied which is updated every 5-15 s. ECRH is applied at a low level of  $P_{\text{EC}} \sim 5$  MW at  $t = 10$  s and then linearly increased to 20 MW at  $t = 80$  s. Time traces of  $I_{\text{pl}}$ ,  $P_{\text{EC}}$ ,  $n_{\text{e,lin-avg}}/n_{\text{GW}}$  and densities for this scan are shown in Fig. 1. For all cases, the thermal energy content  $W_{\text{th}}$  increases from  $\sim 2$  MJ at the beginning of the ramp to  $\sim 17-25$  MJ at  $I_{\text{pl}} = 15$  MA. The internal inductance  $li(3)$  is slowly increasing within a range  $0.70 < li(3) < 0.76$  except for the case at low DT gas puff rate  $\Gamma_{\text{DT,neut}} = 3 \cdot 10^{21}/\text{s}$  (for which  $li(3)$  is decreased to  $\sim 0.70$  at  $I_{\text{pl}} = 15$  MA) which is affected by a significant reduction of the inwards diffusion of the edge induced current that is caused by the following causality chain: low  $\Gamma_{\text{DT,neut}} \rightarrow$  lower core density  $\rightarrow$  reduced electron-ion heat exchange  $\rightarrow$  increased edge electron temperature  $\rightarrow$  reduced edge resistivity. To maintain a constant Greenwald density fraction, the DT gas puff rate needs to be increased with plasma current. Due to the curvature pinch term in the BgB model, the core plasma is slightly peaked. The absolute value of the density scales essentially with the density at the separatrix, which in turn is determined by the applied DT gas puff rate  $\Gamma_{\text{DT,neut}}$ , the heat flux to the separatrix  $P_{\text{sep}}$ , the plasma edge impurity composition and the pump efficiency. In these simulations, the impurity content is very low, with  $Z_{\text{eff}} \sim 1.1$  in the early ramp-up phase and even lower  $Z_{\text{eff}}$  later on due to enhanced fuelling by DT gas injection. Divertor conditions are controlled to avoid any significant release of W by sputtering, without any need for impurity seeding by Ne, and the He ash source due to fusion reactions remains negligible during ramp-up. In this phase the plasma is only contaminated by a small amount of Be that is released at the main chamber wall. As discussed in [Romanelli NF 2015], predictions for the separatrix density are more optimistic at lower  $Z_{\text{eff}}$  for a given  $\Gamma_{\text{DT,neut}}$  and input power  $P_{\text{AUX}}$ . The predictions for  $n_{\text{sep}}$  obtained by JINTRAC at the end of current ramp-up, when comparable SOL transport conditions are achieved, are in good agreement with recent SOLPS-derived scalings suggested in [Pacher JNM 2015] for a pure gas fuelled plasma (cf. Table 1) except for the case with application of a low DT gas puff rate  $\Gamma_{\text{DT,neut}} = 3 \cdot 10^{21}/\text{s}$  for which a normalised

neutral pressure at the entrance of the private flux region  $\mu \sim 0.10$  is achieved that appears to lie outside the range of validity of the scalings (cf. Fig. 1e in [Pacher JNM 2015]).

As the divertor is already predicted to be close to fully detached conditions for the maximum gas puff rates applied in this scan, giving  $n_{e,\text{lin.-avg.}}/n_{\text{GW}} \sim 25\%$ , observations from [Belo EPS 2015, Romanelli NF 2015, Militello-Asp NF 2015] are confirmed that it may be difficult to increase the density in L-mode to access the NB shine-through limit  $n_{\text{NB,sh.-thr.}}$  for DT plasmas by application of gas puff alone even at higher  $I_{\text{pl}}$ . According to [Polevoi NF 2013],  $n_{\text{NB,sh.-thr.}} \sim 3.0 \cdot 10^{19}/\text{m}^3$  with a shine-through power density limit on the inner wall, considering additional shine-through armour, of  $p_{\text{NB,shine-through}} < 4 \text{ MW}/\text{m}^2$  for a DT plasma at  $Z_{\text{eff}} = 1.96$ . As the shine-through limit decreases with increasing impurity content,  $n_{\text{NB,sh.-thr.}} > 3.0 \cdot 10^{19}/\text{m}^3$  for the low  $Z_{\text{eff}}$  plasmas considered in the current ramp up simulations presented here. Despite the dependency of  $n_{\text{NB,sh.-thr.}}$  on the impurity contamination, it might be easier to reach the NB shine-through limit by gas puff application in low  $Z_{\text{eff}}$  plasmas, as the positive dependence of  $n_{\text{sep}}$ , which determines the core density, on  $Z_{\text{eff}}$ , may be more important. Moderate pellet fuelling might in any case be desirable before NB heating can be applied.

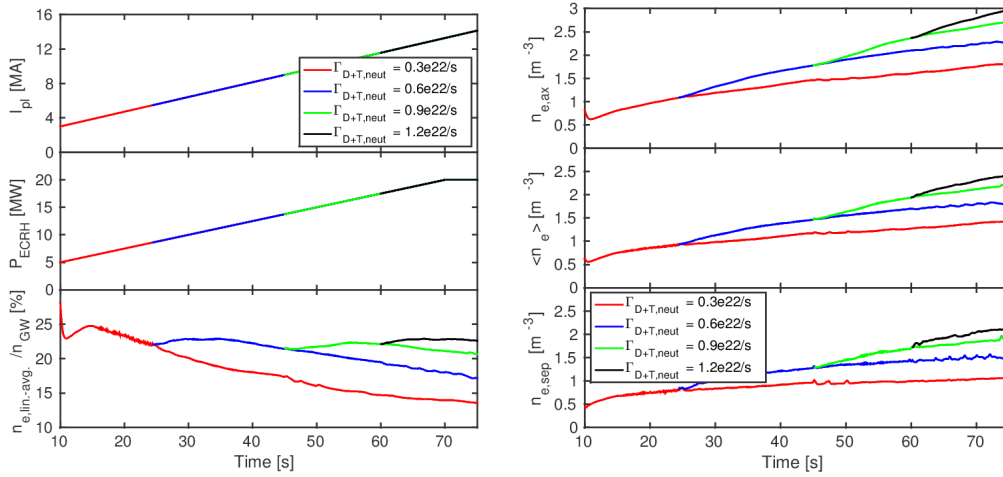


**Figure 1.** Left, from top to bottom: time evolution of plasma current, EC power and Greenwald density fraction, right: time evolution of central, volume-averaged and separatrix electron density during the current ramp-up from 3-15MA for the scan in nominal DT gas puff rates.

**Table 1.** Comparison of electron density at the separatrix as predicted by JINTRAC in the current ramp-up scan simulations with scalings derived from SOLPS scans ([Pacher JNM 2015], equ. 1 and 3) for varying  $\Gamma_{\text{DT,neut}}$  in quasi-stationary conditions at  $I_{\text{pl}} = 15 \text{ MA}$ ,  $P_{\text{AUX}} = 20 \text{ MW}$ ,  $Z_{\text{eff}} \sim 1.0$ .

DT gas puff rate [ $10^{22}/\text{s}$ ]	$n_{e,\text{sep,SOLPS scaling}}$ [ $10^{19}/\text{m}^3$ ]	$n_{e,\text{sep,JINTRAC}}$ [ $10^{19}/\text{m}^3$ ]	$n_{e,\text{sep,JINTRAC}}/n_{e,\text{sep,SOLPS scaling}}$ [%]
0.3	0.66	1.07	162
0.6	1.74	1.55	89
0.9	2.08	1.90	91
1.2	2.19	2.15	98

### 3.1.2 Scan in heating scheme and current ramp rate

In this heating and current ramp-rate scan, a target Greenwald density fraction is prescribed that is maintained by the application of a feedback controlled DT gas puff. The target density fraction is set low enough to avoid strong detachment but still large enough to keep the ion temperature below  $\sim 5 \text{ eV}$  on the targets at the location of maximum ion current density in order to avoid a significant release of W. During current ramp-up, the target Greenwald

density fraction is adjusted in a stepwise way and kept constant for intervals of  $\sim 2$ -3 MA in terms of the increase in plasma current to achieve an optimal density evolution.

The following three cases have been investigated:

A1. Medium  $dI_p/dt$ , adaptive heating scheme:

- $I_p$  linearly ramped from 3 MA to 15 MA between  $t = 10 - 70$  s
- Ohmic heating in early ramp-up phase ( $I_p = 3 - 5$  MA)
- $I_p = 5 - 10$  MA: linear increase in ECRH power from 0 MW to 20 MW
- $I_p > 10$  MA: 20 MW of ECRH power

A2. Medium  $dI_p/dt$ , linearly increased ECRH power:

- $I_p$  linearly ramped from 3 MA to 15 MA between  $t = 10 - 70$  s
- Linear increase in ECRH from 5 MW to 20 MW between  $t = 10 - 70$  s

A3. High  $dI_p/dt$ , linearly increased ECRH power:

- $I_p$  linearly ramped from 3 MA to 15 MA between  $t = 10 - 50$  s
- Linear increase in ECRH from 5 MW to 20 MW between  $t = 10 - 50$  s

The plasma evolution for these three cases is shown in Figs. 2-3.

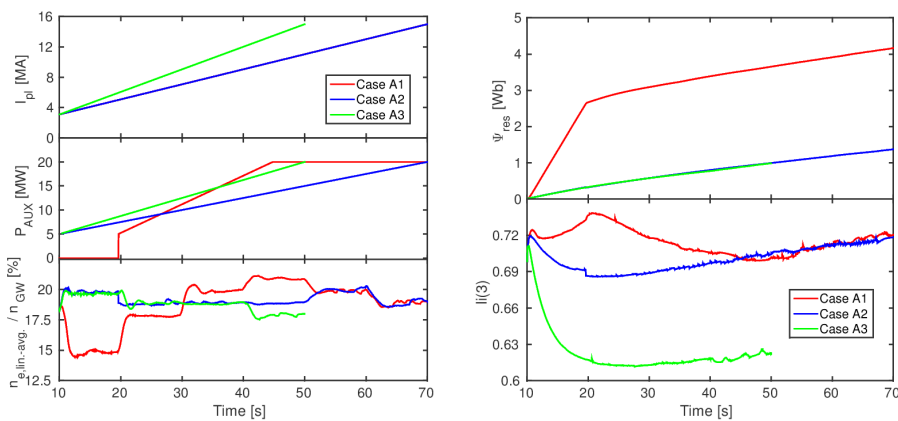


**Figure 2.** Left: Time evolution of plasma current, auxiliary power and Greenwald density fraction (from top to bottom), right: time evolution of resistive poloidal flux consumption (top) and internal inductance  $li(3)$  (bottom), during the current ramp-up from 3-15MA for the scan in heating scheme and current ramp rate.

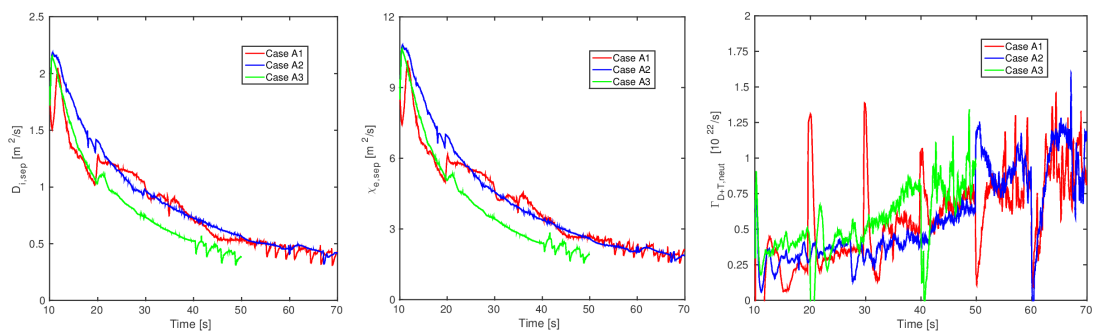


**Figure 3.** Time evolution of particle (left) and heat diffusivities (middle) at the separatrix and the D+T gas puff rate (deviation from actual puff rates due to applied partial coupling scheme not considered) during the current ramp-up from 3-15MA for the scan in heating scheme and current ramp rate.

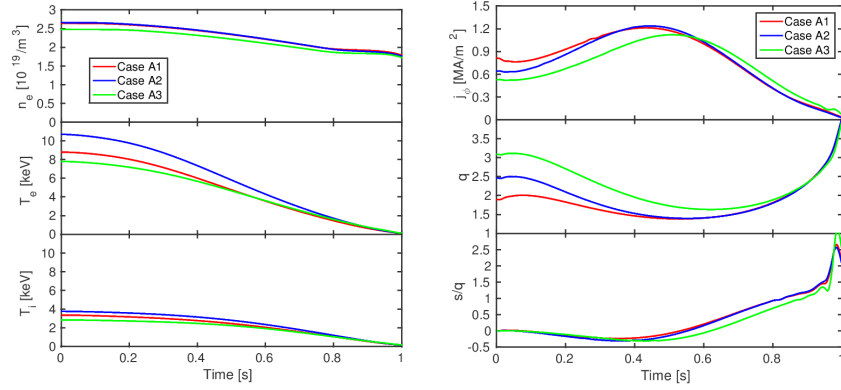


**Figure 4.** Final plasma profiles when the current has reached 15MA for current ramp-up from 3-15MA for the scan in heating scheme and current ramp rate. Left, from top to bottom: electron density, electron temperature, ion temperature. Right, from top to bottom: toroidal current density, safety factor, ratio between magnetic shear and safety factor.

It is very significant to note that a ramp in current to  $I_{pl} = 15$  MA respecting PF coil current, fuelling, heating and divertor operational constraints appears to be feasible. By operation at a low density in the order of  $\sim 20\%$  of the Greenwald density limit for moderate auxiliary heating in the order of  $\sim 10$  MW, simulations indicate that applied gas fluxes are low enough to avoid detachment but high enough to keep the ion temperature on the divertor targets in the vicinity of the strike points below the critical level for W sputtering. The operational window of achievable densities with gas puff only, which was explored by variation of the feedback control target for  $n_{e,lin-avg.}/n_{GW}$  in complementary simulations for intervals in  $I_{pl}$  of  $\sim 2-3$  MA, seems to be quite narrow for a given level of  $P_{AUX}$  ( $\pm \sim 5\%$  of the Greenwald density). It should be noted that predictions of the achievable density range by gas puff only depend on SOL transport assumptions as demonstrated e.g. in [Belo EPS 2015, Romanelli NF 2015]. According to simulation results, gas puff rates must increase by a factor of  $\sim 4$  when  $I_{pl}$  is ramped up from 3 MA to 15 MA to maintain a constant Greenwald density limit of  $\sim 20\%$ . In absolute values, optimum DT puff rates may be in the order of  $\sim 0.5-1.0 \cdot 10^{22}/s$  (cf. Fig. 3).

Achievable densities appear to be particularly low for ohmically heated plasmas ( $< \sim 15\%$  of  $n_{GW}$ ) at low currents. Although  $n_{GW}$  is lower for low  $I_{pl}$ , the connection length is increased in the SOL, and perpendicular diffusion is predicted to be enhanced at higher safety factor (cf. Fig. 3) causing an increased spread in heat flux over the divertor target. To avoid detachment, the density thus needs to be considerably reduced by  $\sim 25\%$  for a low heat flux from the core in the early ramp-up phase for Case A1 as compared to Cases A2-3. A gradual transition from purely Ohmic to ECRH assisted heating within a few seconds may be desirable to keep detachment and W sputtering under control. It may be advisable to maintain at least a low level of auxiliary heating of  $P_{AUX} \geq \sim 10$  MW during the entire current ramp-up phase for improved density control, but also for the reduction of resistive poloidal flux losses that may limit the burn duration in the flat-top phase (cf. [Hogewij NF 2013, Parail NF 2013]). Resistive losses may be increased by  $\sim 0.25$  Wb/s with purely Ohmic heating (cf. Fig. 2).

Operation at low density during current ramp-up with EC heating has a noticeable impact on current diffusion, as the resistivity is comparably low in these conditions. The current density profile is thus predicted to remain hollow at the end of ramp-up at  $I_{pl} = 15$  MA (cf. Fig. 4) even for cases with moderate to low current ramp rates (i.e. for a total ramp duration of  $\sim 70-80$  s), giving low  $s/q$  that may be unfavourable for plasma confinement in the early flat-top phase as described in [Parail NF 2013].

Comparing the ramp-up simulation at higher  $dI_{pl}/dt$  (Case A3) with the simulations at medium  $dI_{pl}/dt$  (Cases A1-2), a modest reduction in flux consumption is predicted over the

shorter ramp up time, but other challenges may become important: enhanced core transport in the flat-top phase caused by a further reduction in  $s/q$ ; and a significant reduction in internal inductance  $li(3)$  which may reach the lower limit of  $li(3) \sim 0.6$  for plasma shape control by PF coil current adjustment [Mattei FED 2009] (cf. Fig.2).

Regarding fuelling conditions, differences in accessible  $n_{e,lin.-avg.}/n_{GW}$  for cases at low vs. high current ramp rate appear to be modest, though there is a slight hint that the achievable ratio  $n_{e,lin.-avg.}/n_{GW}$  might decrease for increased  $dI_{pl}/dt$ . This result can be naturally explained by the need to increase the gas puff rate in order to achieve the same  $n_e/n_{GW}$  at higher  $dI_{pl}/dt$  while the limit in gas puff rates to avoid detachment might be independent of  $dI_{pl}/dt$ .

### 3.2 L-H transition and density ramp at 15 MA

The current ramp-up simulation Case A1 as described in Subsection 3.1.2 has been continued for the early flat-top phase at  $I_{pl} = 15$  MA. The simulation is restarted to allow for a different impurity configuration, switching from Be to He and (bundled) Ne. As the density is still below the NB shine-through limit of  $n_{NB,sh.-thr.} \sim 3.0 \cdot 10^{19}/m^3$  [Polevoi NF 2013] at the end of current ramp-up, small pellets (with radius  $r_p = 2$  mm for spherical shape, corresponding to  $N_p \sim 2.1 \cdot 10^{21}$  particles per pellet) are injected until a line-average density of  $n_{e,lin.-avg.} \sim 3 \cdot 10^{19}/m^3$  is obtained. Full NB power of 33 MW is then applied and the transition to H-mode is triggered. The density is then roughly maintained at a constant level to assure a fast increase in pedestal pressure and in central ion temperature such that the net heat flux can be kept above the L-H transition power threshold due to the increase in alpha heating as described in [Loarte NF 2013, Koechl NF 2017]. After a few seconds, the density is then gradually ramped by standard ITER fuelling size pellets ( $r_p = 2.86$  mm,  $N_p \sim 6.1 \cdot 10^{21}$ ) to a target density of  $n_{e,lin.-avg.} \sim 10^{20}/m^3$  using pellet injection feedback control with the aim of reaching a stationary H-mode in the burning regime at  $Q_{fus} \sim 10$ . To ensure that heat flux densities to the divertor remain below the target of  $10$  MW/m<sup>2</sup>, the Ne puff rate is strongly increased before stationary ELMy H-mode conditions at high  $Q_{fus}$  are reached.

The following simulation cases with NB heating applied at  $t > \sim 72.5$  s have been considered:

- B1. Density maintained at a low level for  $\sim 5$  s, then slowly ramped up to  $n_{e,lin.-avg.} \sim 10^{20}/m^3$  by pellets within  $\sim 30$  s.
- B2. Density maintained at a low level for  $\sim 5$  s, then quickly ramped up to  $n_{e,lin.-avg.} \sim 10^{20}/m^3$  by pellets within  $\sim 10$  s.
- B3. Density maintained at a low level for  $\sim 12$  s, then quickly ramped up to  $n_{e,lin.-avg.} \sim 10^{20}/m^3$  by pellets within  $\sim 10$  s.
- B4. Density increased by gas fuelling only, no pellet injection.

The plasma evolution for these three cases is shown in Figs. 5-9.

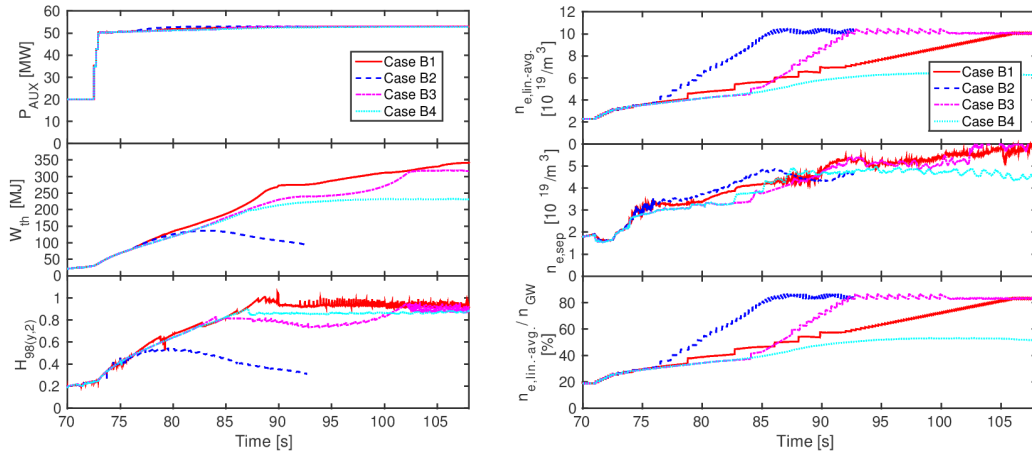


**Figure 5.** Left: Time evolution of auxiliary power, thermal energy content and  $H_{(98,y2)}$  factor, right: time evolution of line-averaged electron density, electron density at the separatrix and  $n_{e,lin.-avg.}/n_{GW}$  (from top to bottom), from the end of ramp-up at 15 MA, for Cases B1-B3 as described in Subsection 3.2.

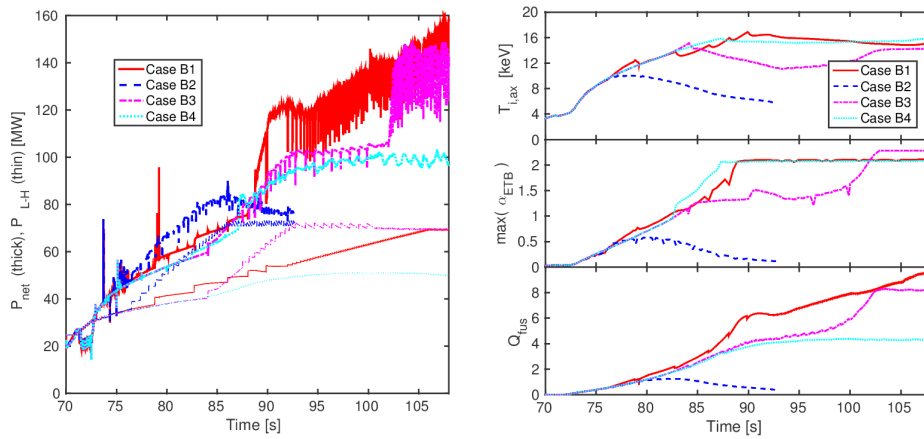


**Figure 6.** Left: Time evolution of net power (thick lines) vs. L-H transition power threshold (thin lines), right: time evolution of the ion temperature on axis (top), the maximum normalised pressure gradient in the ETB (middle) and fusion Q (bottom) from the end of ramp-up at 15 MA, for Cases B1-B3 as described in Subsection 3.2.

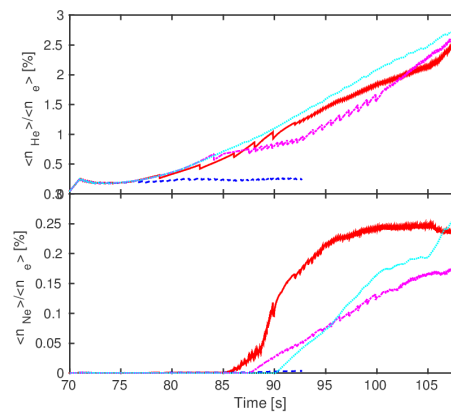


**Figure 7.** Time evolution of He (top) and Ne (bottom) core concentration from the end of ramp-up at 15 MA, for Cases B1-B3 as described in Subsection 3.2.

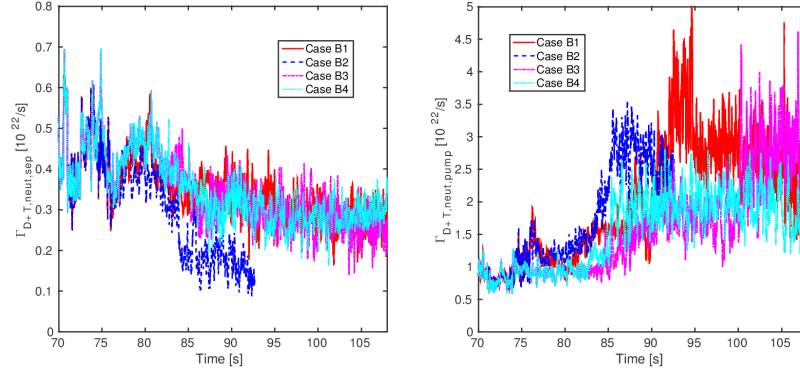


**Figure 8.** Time evolution of D+T neutral influx at the separatrix (left) and D+T pump rate (right) from the end of ramp-up at 15 MA, for Cases B1-B3 as described in Subsection 3.2.

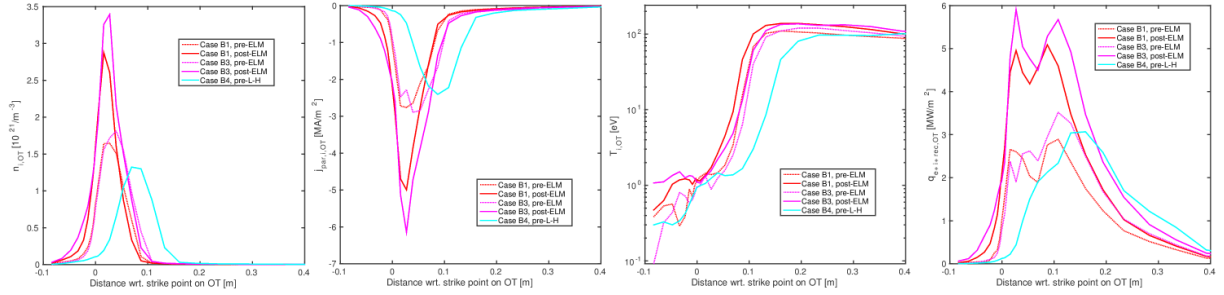


**Figure 9.** Profiles of ion density, parallel current density, ion temperature and power density (from left to right) at the and outer target for Cases B1 (red) and B3 (magenta) before (dashed) and after the onset of ELMs (solid), and for Case B3 before back transition to L-mode (blue) as described in Subsection 3.2.

As the ratio between the net power flux crossing the separatrix  $P_{\text{net}}$  and the L-H transition threshold  $P_{\text{L-H}}$  is expected to stay close to 1.0 before the onset of significant  $P_{\alpha}$ , the density needs to be kept at a low level after the L-H transition until the fusion reaction process sets in. As soon as alpha heating becomes significant and  $P_{\text{net}} / P_{\text{L-H}}$  is increased, the density can be ramped up by pellets. If there is no delay between the L-H transition and the density ramp or the density is increased too quickly,  $P_{\text{net}} / P_{\text{L-H}}$  may approach or even drop below the level of 1.0 and the plasma might remain in a degraded type-III ELMy H-mode like regime or eventually jump back to L-mode (cf. [Loarte NF 2013, Koechl NF 2017]). To assure a fast increase in alpha heating, the density needs to be ramped such that the ion temperature in the core remains well above a critical level of  $T_{i,\text{crit}} \sim 10$  keV for the cross section of the DT reaction to be sizeable [Koechl NF 2017].

The requirement for a delayed and gradual ramp in density needs to be reconciled with the need to reduce flux consumption to allow for a long steady state which would require the transition to a stationary burning H-mode regime at  $Q_{\text{fus}} \sim 10$  to be achieved as quickly as possible. Simulation results indicate that it might be optimal to maintain the density at a low level for  $\sim 5$ -10 s after the L-H transition and then to apply a ramp in density by pellets to a target Greenwald density fraction of  $\sim 60$ -90% within  $\sim 10$ -20 s, confirming results from more detailed transition scans by means of core+edge transport modelling in [Koechl NF 2017].

As another aspect to consider in the early H-mode phase, the pedestal evolves very slowly after the L-H transition due to enhanced transport for  $P_{\text{net}} / P_{\text{L-H}}$  staying close to 1.0, reaching an ELM free H-mode period in the order of  $\sim 10$  s. In order to achieve a transition to a burning regime at  $Q_{\text{fus}} \sim 10$  as fast as possible, the ramp in density by pellets may need to be already started before the pedestal is fully developed. This requirement must however be balanced with the need to maintain a high ratio between the ion temperature and ion density gradients in the pedestal  $dT_{i,\text{ped}}/dn_{i,\text{ped}}$  in the transition to high  $Q_{\text{fus}}$  for the minimisation of core impurity

contamination [Dux PPCF 2014, Koechl NF 2017], which may be more difficult to achieve in the early transition phase with enhanced pellet fuelling.

Regarding divertor control by impurity seeding, the simulations indicate that no Ne puff might be required for the first few seconds after the L-H transition when the density is maintained at a low level, the plasma is still in ELM free H-mode phase and  $Q_{\text{fus}}$  remains low. However, Ne seeding may need to be applied before the pedestal is fully developed to keep the maximum heat flux on the divertor targets below  $10 \text{ MW/m}^2$  when the (time-averaged) heat flux crossing the separatrix suddenly increases by  $\sim 20\text{-}25 \text{ MW}$  within the energy confinement time  $\tau_E \sim 2.5 \text{ s}$  at the start of the ELMy H-mode phase. This may be a challenge, as a time delay needs to be considered for the establishment of the required Ne concentration in the SOL for the following reasons: a significant fraction of puffed Ne initially is lost into the confined region until quasi-stationary conditions are achieved for the Ne density in the core; it takes a few hundred milliseconds for Ne gas to arrive in the plasma vessel [Bonnin NME 2017]. Our simulations assume an instantaneous response of the Ne arriving in the SOL to changes in the requested Ne puff rate, which may be overoptimistic.

To maintain the maximum heat flux on the divertor targets below  $10 \text{ MW/m}^2$  and to keep the ion temperature in vicinity of the strike points below  $\sim 5 \text{ eV}$  to minimise W sputtering, a DT gas puff rate in the order of  $\sim 1.0\text{-}1.5 \cdot 10^{22}/\text{s}$  may need to be applied in the low density phase after the L-H transition. Later on, when the density is ramped up by pellets, the DT gas puff rate may need to be increased to  $\sim 2.0 \cdot 10^{22}/\text{s}$  to accommodate enhanced heat fluxes that are caused by the increase in alpha heating. The DT gas puff rate would need to be reduced again as soon as Ne seeding is applied. The effect of Ne seeding is enhanced at higher DT gas puff rates, as Ne can be kept closer to the divertor plates so that core contamination by Ne can be reduced at higher SOL densities. In stationary burning conditions, required Ne puff rates may be in the order of  $\sim 10^{19}/\text{s}$ .

### 3.3 L-H transition and density ramp at $\sim 10\text{-}12 \text{ MA}$

The current ramp-up simulation Case A2 as described in Subsection 3.1.2 has been continued from  $I_{\text{pl}} \sim 9 \text{ MA}$ , including He and bundled Ne impurities. As for the L-H transition cases at flat-top current that have been described in Subsection 3.2, small ( $r_p = 2 \text{ mm}$ ,  $N_p \sim 2.1 \cdot 10^{21}$ ) pellets need to be injected until a line-average density of  $n_{e,\text{lin.-avg.}} \sim 3 \cdot 10^{19}/\text{m}^3$  is obtained to ensure that NB shine-through losses are acceptably low, although this may lead to temporary divertor detachment while the auxiliary power is still limited to EC heating, which may be more difficult to avoid at lower  $I_{\text{pl}}$  due to: increased edge heat conductivities ( $q^2$  dependence of Bohm transport coefficients) and increased SOL connection lengths at higher  $q$ . Full NB power of  $33 \text{ MW}$  is then applied and the transition to H-mode is triggered. NB sources are modelled by ASCOT [Heikkinen PoP 1995, Hirvijoki CPC 2014] in these cases to take the beam particle thermalisation time into account which may delay the transition to H-mode by a few seconds for low initial  $P_{\text{net}}/P_{\text{L-H}}$ . After the start of NB heating, the density is then roughly maintained at a constant level in an attempt to achieve partial divertor re-attachment and a fast increase in pedestal pressure and in central ion temperature so that the net heat flux can be kept above the L-H transition power threshold and alpha heating develops in the core. After a delay of  $\sim 10 \text{ s}$ , the density is then gradually ramped by standard ITER size pellets ( $r_p = 2.86 \text{ mm}$ ) within  $\sim 30 \text{ s}$  using pellet injection feedback control to access a stationary high quality H-mode burning regime.

The plasma evolution for the simulation with an early L-H transition is shown in the figures below in green. For comparison, simulation results for Case A2 from the current ramp-up scan in Subsection 3.1.2 (current ramp-up with plasma maintained in L-mode) are also shown in blue.

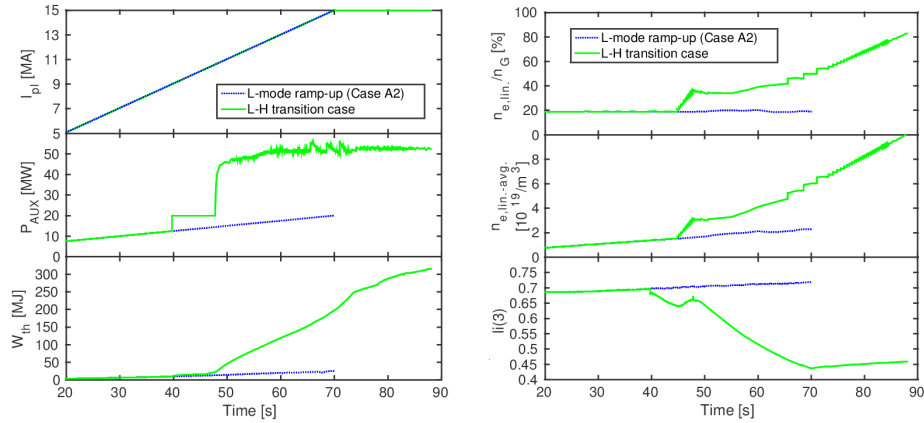


**Figure 10.** Left: Time evolution of plasma current (top), auxiliary power (middle) and thermal core energy content (bottom), right: time evolution of Greenwald density fraction (top), line-averaged electron density (middle) and internal inductance  $li(3)$  for an early L-H transition at  $I_{pl} \sim 10$  MA (green colour), compared to a similar current ramp-up configuration without L-H transition (blue colour, Case A2 from the Subsection 3.1.2).

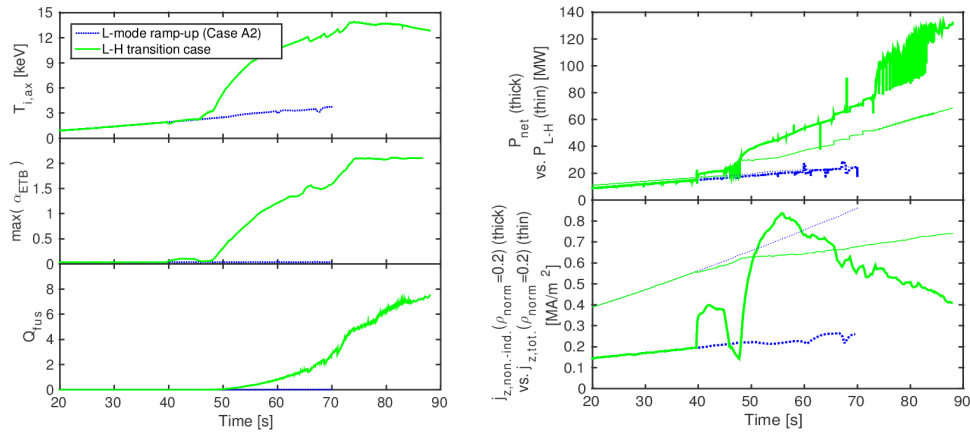


**Figure 11.** Left: Time evolution of the ion temperature on axis (top), the maximum normalised pressure gradient in the ETB (middle) and fusion Q (bottom), top right: time evolution of the net power (thick) vs. the L-H transition power threshold (thin), bottom right: time evolution of the non-inductive (thick) vs. total (thin) current density in the plasma centre ( $\rho_{norm} = 0.2$ ), for an early L-H transition at  $I_{pl} \sim 10$  MA (green colour), compared to a similar current ramp-up configuration without L-H transition (blue colour, Case A2 from the Subsection 3.1.2).

The simulation confirms that the transition to high  $Q_{fus}$  may be more difficult to achieve for an early L-H transition during the current ramp-up phase. Confinement properties may be less favourable at lower current, as transport is predicted to increase at higher  $q$  and lower ratio between shear and  $q$  that is caused by a hollow current density profile at the time of the L-H transition and decelerated penetration of edge-induced current towards the core when the plasma is in H-mode (cf. [Citrin NF 2012, Parail NF 2013]). The impact of  $s/q$  on peripheral core plasma transport is well reproduced in these simulations using the GLF-23-retuned version of the BgB model. This is due to the  $q^2$  dependence in the Bohm term of the BgB model, which mimics reasonably well the transport dependence on  $s/q$  obtained with GLF-23 for ITER high current baseline H-mode plasmas.

Before the L-H transition, the density needs to be ramped by pellets to the NB shine through limit starting from a much lower initial density level. After the L-H transition, the ion temperature in the core needs to be increased to  $> 10$  keV to initiate the fusion process starting from a much lower initial temperature. Furthermore, it is more difficult to achieve and maintain high core temperatures at lower currents, as the MHD limit for the pedestal pressure  $p_{ped}$  is significantly lower at lower currents ( $p_{ped} \propto I_{pl}$  [Polevoi NF 2015]).

Required gas puff rates to maintain the divertor targets below  $10 \text{ MW/m}^2$  and to keep the ion temperature in the vicinity of the strike points below  $\sim 5 \text{ eV}$  during the first few seconds after the L-H transition might be lower if the L-H transition is triggered at reduced  $I_{p1}$  ( $\Gamma_{DT} \sim 0.5-1.0 \cdot 10^{22}/\text{s}$  for the early L-H transition case). This is due to increased transport at higher  $q$  and larger connection lengths in the SOL, yielding an increased spread in heat flux along the divertor targets.

If the current ramp rate is maintained constant after an early L-H transition, the internal inductance could drop to very low values  $li(3) < \sim 0.6$  (cf. Fig. 10). This might be challenging for plasma shape control [Mattei FED 2009, Parail NF 2013]. If the current ramp rate in H-mode is reduced to maintain  $li(3) > 0.6$ , the current ramp up time might increase to a few hundreds of seconds which would significantly reduce the maximum burn duration at high  $Q_{fus}$ . Furthermore plasma transport may be significantly degraded in plasmas where the current ramp continues in H-mode for an extended period determined by the current diffusion time due to differences in the safety factor profile shape triggered by a delayed inwards current diffusion. Although these findings have already been described in [Parail NF 2013], the simulation results presented in this paper for an early L-H transition suggest that they may deserve more attention than previously estimated. This is because the internal inductance is predicted to be already close to the threshold  $li(3) \sim 0.6$  before the start of the L-H transition in the new simulations due to an earlier start of the full bore diverted configuration, application of more auxiliary heating power starting at an earlier time and operation at lower  $n_{e,lin.-avg.}/n_{GW}$  as compared to the simulations shown in [Parail NF 2013]. In addition, the delay in the establishment of good quality H-mode conditions due to  $P_{sep}$  staying close to  $P_{L-H}$  after the L-H transition has not been taken into account previously. New strategies are clearly required to maintain a sufficiently high value of  $li(3)$  after an early L-H transition.

It is worth noting that the non-inductive current fraction can become significant ( $\sim 40-50\%$ ) in the early phase after the L-H transition when the density is kept low. Near the magnetic axis, it can happen that the non-inductive current density exceeds the total current density triggering the appearance of a negative voltage in the core which could give rise to current hole formation (cf. Fig. 11).

### 3.4 Complete transition from early current ramp-up to high $Q_{fus}$

Fig. 12 summarises a subset of our simulations of the plasma evolution from early current ramp up to high  $Q_{fus}$ . Fig. 12 demonstrates that the main criteria for the protection of the divertor ( $\max(q_{target}) < 10 \text{ MW/m}^2$ ,  $T_{i,jmax,OT} < \sim 5 \text{ eV}$ ) are reasonably well fulfilled at all times. JINTRAC simulation results thus indicate that viable plasma scenario configurations to approach the ITER target of  $Q_{fus} \sim 10$  can be conceived with the available fuelling actuators, with plasma evolution successfully controlled to respect major operational limits.

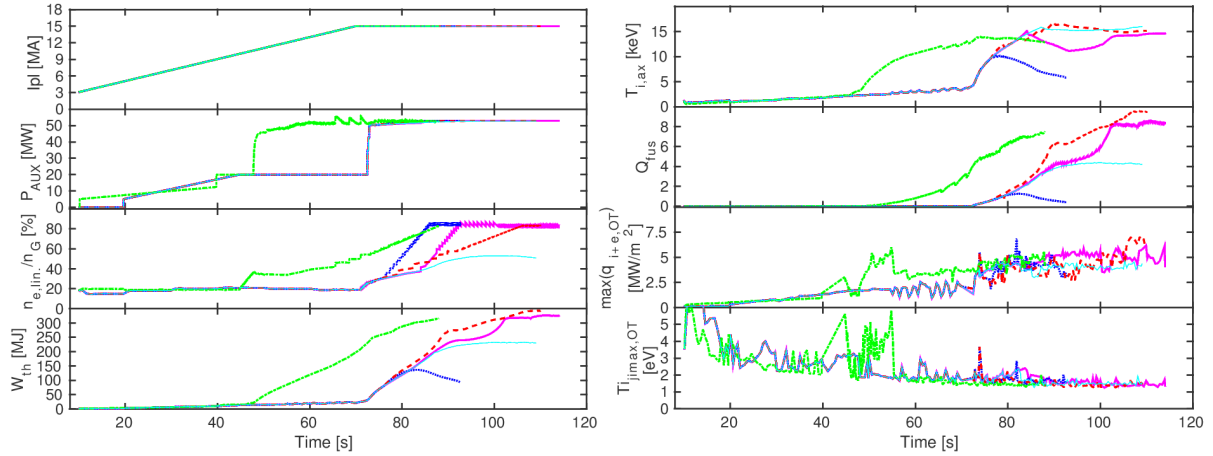


**Figure 12.** Left, from top to bottom: Time evolution of plasma current, auxiliary power, Greenwald density fraction, thermal energy content, right, from top to bottom: time evolution of ion temperature on axis, fusion  $Q$ , the maximum power density at the outer target (considering power transferred by electrons, ions and due to recombination) and ion temperature at the outer target location with the maximum absolute value of ion current density, from early current ramp-up at 3 MA to good quality H-mode for the following cases: red dashed: Case A1 from Subsection 3.1.2 and Case B1 from Subsection 3.2, blue dotted: Case A1 from Subsection 3.1.2 and Case B2 from Section 3.2, magenta solid: Case A1 from Subsection 3.1.2 and Case B3 from Subsection 3.2, green dash-dotted: Case A2 from Subsection 3.1.2 until  $I_{pl} \sim 9$  MA, followed by the early L-H transition case from Subsection 3.3, cyan thin solid: Case A1 from Subsection 3.1.2 and Case B4 from Subsection 3.2.

#### 4. Transition from stationary high $Q_{fus}$ regime to late current ramp-down phase

##### 4.1. Simulation of stationary H-mode at $Q_{fus} \sim 10$ with discrete pellet fuelling and including He transport

The JINTRAC simulations for gas and pellet fuelled high  $Q_{fus}$  H-mode plasmas at  $I_{pl} = 15$  MA and  $B_0 = 5.3$  T at  $P_{AUX} = 53$  MW (33 MW NB + 20 MW EC power) with W target that have been presented in Subsection 3.2 have been repeated at a fixed D+T gas puff rate of  $\Gamma_{DT,neut} = 10^{22}/s$  with Ne seeding. He and (bundled) Ne impurity transport are taken into account. Ne seeding is adjusted by feedback control (assuming ideal instantaneous feedback control with a zero feedforward control puff rate) in order to maintain a Ne radiation level in the SOL and private flux region of  $\sim 30$  MW, giving an averaged Ne concentration in the SOL and private flux region of  $\sim 0.5\%$ . Pellets with a 1:1 D-T mixture and a size of  $r_p \sim 0.28$  mm ( $N_p \sim 6.1 \cdot 10^{21}$ ) are injected at a speed of  $v_p = 300$  m/s from the upper HFS [Baylor SOFE 2015]. The pellet injection frequency is adjusted by a feedback control scheme in order to maintain a line-averaged electron density of  $\sim 1.0-1.05 \cdot 10^{20}/m^3$ . He is produced by fusion reactions in the core. The simulation is continued for several tens of seconds until stationary conditions are approached for the He density in the core and edge regions.

Simulation results are shown in the Figs. 13-16:

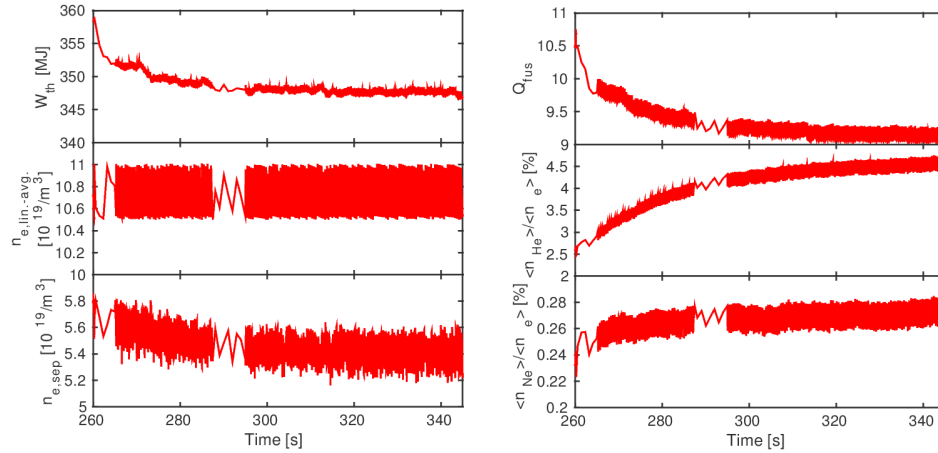


**Figure 13.** Left: Time evolution of thermal energy content, line-averaged electron density and electron density at the separatrix, right: time evolution of fusion  $Q$ , the He core concentration and the Ne core concentration (from top to bottom) for the pellet and gas fuelled high  $Q_{\text{fus}}$  D+T H-mode plasma described in Section 4.1.

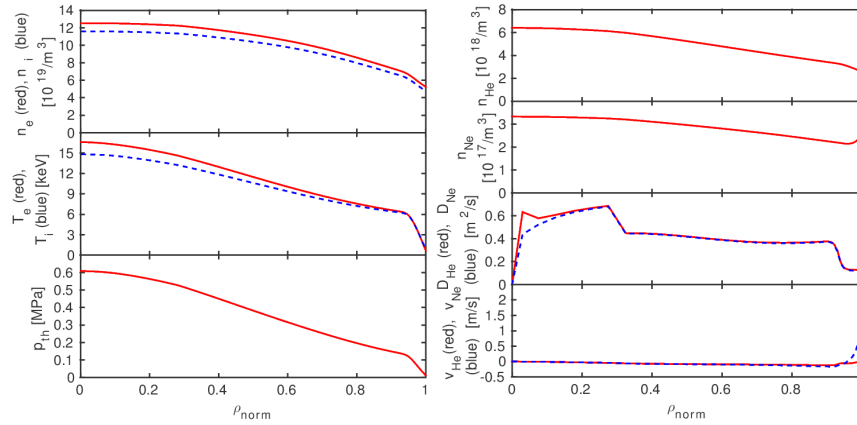


**Figure 14.** Left: Plasma profiles of electron (red, solid) and ion (blue, dashed) density (top), temperature (middle) and thermal pressure (bottom), right: plasma profiles of He density, Ne density, He (red, solid) and Ne (blue, dashed) diffusivity and convection velocity (from top to bottom), at  $t \sim 318.8$  s (close to stationary conditions) for the pellet and gas fuelled high  $Q_{\text{fus}}$  D+T H-mode plasma described in Section 4.1.

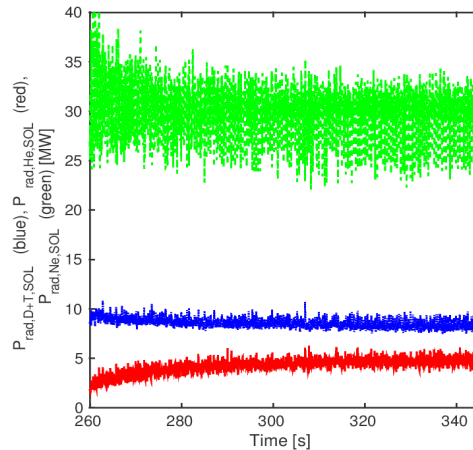


**Figure 15.** Time evolution of D+T (blue, dotted), He (red, solid) and Ne (green, dashed) induced radiation in the SOL and private region for the pellet and gas fuelled high  $Q_{\text{fus}}$  D+T H-mode plasma described in Section 4.1.

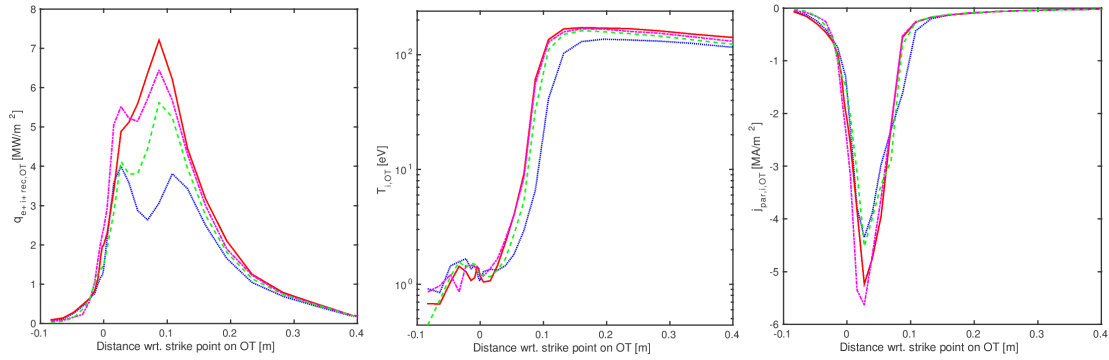


**Figure 16.** Power flux density (left, including power from electrons, ions and recombination), ion temperature (middle) and parallel current density (right) at the outer target at various time instants during a pellet injection cycle for the pellet and gas fuelled high  $Q_{\text{fus}}$  D+T H-mode plasma described in Section 4.1.

According to simulation results, the maximum power density on the inner and outer targets,  $\max(q_{\text{IT}})$  and  $\max(q_{\text{OT}})$ , can be maintained below  $10 \text{ MW/m}^2$  with the applied D+T and Ne puff rates (cf. Fig. 16). It should be noted however that the power density on the inner target is predicted to be similar or sometimes even locally exceed the power density on the outer target, and that cross-field drifts in the SOL have not been considered. If the latter were taken into account, an asymmetric heat deposition pattern would be expected that might give  $\max(q_{\text{OT}})$  in excess of the estimates obtained in these simulations. It may therefore be possible that the condition  $\max(q_{\text{OT}}) < 10 \text{ MW/m}^2$  is not always fulfilled for the plasma configuration considered here if SOL drifts are taken into account.

Due to discontinuities in the assumed radial dependency of perpendicular transport coefficients from the modelled extension of the ETB into the SOL, the SOL heat flux does not decay exponentially. It is therefore not possible to determine a reliable heat decay width  $\lambda_q$  from these simulations that can be directly compared to scalings such as [Eich NF 2013]. However, local estimates of  $\lambda_q$  that are applicable only for the very near SOL region can be inferred. For stationary high  $Q_{\text{fus}}$  flat-top conditions, values for  $\lambda_q$  in the order of  $\sim 1 - 2 \text{ mm}$  are obtained in agreement with estimates for Scan 1 in Table 1 in [Romanelli NF 2015]. Although these estimates are in rough agreement with the scaling from Eich et al. [Eich NF 2013], it should be noted that local estimates of  $\lambda_q$  for exterior SOL regions are significantly higher. Compared to recent gyrokinetic projections for the heat decay width for  $Q_{\text{fus}} = 10$  plasmas in ITER [Chang NF 2017] giving  $\lambda_q = \sim 5-6 \text{ mm}$  due to enhanced heat transport driven by non-linear edge turbulence effects, the estimates obtained in the JINTRAC simulations presented here can nevertheless be considered as a rather conservative approach for the modelling of divertor control capabilities. Perpendicular transport in the near SOL is assumed to be mainly neoclassical due to the assumption of the extension of the ETB into the SOL, giving predictions of  $\max(q_{\text{OT}})$  that may be in the upper range of expectations due to a reduced spread in heat flux on the target plates in these conditions.

The profile shape of the predicted heat flux on the target plates sometimes exhibits a double peak, which may be particularly pronounced on the inner target. Typically, this double peak is the consequence of different locations of the maximum heat flux density due to ion and electron heat conduction and convection and due to particle recombination at the target plates. The peak position of the latter corresponds to that of the parallel ion flux density which is located in close proximity to the strike point. In addition, the discontinuity of the perpendicular SOL transport coefficients in the near SOL in H-mode due to the extension of the ETB into the SOL is also partly responsible for the formation of two peaks in  $q_{\text{IT}}$  or  $q_{\text{OT}}$ .

To achieve a Ne radiation level in the SOL and private region of  $\sim 30 \text{ MW}$  (cf. Fig. 15), Ne may need to be puffed at a time-averaged puff rate in the order of  $\sim 10^{19}/\text{s}$ .  $T_i$  can be kept below the critical level for W sputtering of  $\sim 5 \text{ eV}$  over a  $\sim 5 \text{ cm}$  wide region near the strike-

point location on the outer target where the absolute ion current density peak is located. Divertor profiles might change considerably immediately after the injection of a pellet. We do not have access to high time resolution results for the post-pellet phase, so cannot comment here on temporary detachment and pellet triggered transient changes in divertor conditions. There are however some hints in Fig. 16 that significant fluctuations in divertor conditions are indeed triggered by the injection of pellets. These transients may present additional challenges for divertor control, and have been investigated in more detail in [Garzotti NF 2019, Wiesen NF 2017].

To maintain the density at a level of  $\sim 85\%$  of the Greenwald density limit, pellets with the standard ITER size need to be injected at a time-averaged frequency of  $\sim 2\text{--}2.5$  Hz which is in line with previous core transport fuelling studies as presented in [L. Garzotti NF 2012].

The He density at the separatrix saturates at  $n_{\text{He,sep}} \sim 2.5 \cdot 10^{18}/\text{m}^3$ , while the He density on axis approaches  $n_{\text{He,ax}} \sim 6 \cdot 10^{18}/\text{m}^3$ , corresponding to a core He peaking factor of  $n_{\text{He,ax}}/n_{\text{He,sep}} \sim 2.4$ . This peaking factor is considerably larger than that obtained in core-only simulations with the GLF-23 transport model [Waltz PoP 1997] with comparable  $n_{\text{He,ax}}$  as described in [Garzotti NF 2019]. This is due to different assumptions for the He core diffusivity: here  $D_{\text{He}}$  is taken to be identical to the diffusivity for main ions with the BgB model retuned to GLF-23 [Garzotti NF 2012] and thus much lower than  $D_{\text{He}}$  as predicted with GLF-23 itself [Garzotti NF 2019]. The He transport assumptions made here are more conservative than assuming the GLF-23 model.

As soon as quasi-stationary conditions are reached, the time-averaged He pump rate becomes identical to the He source rate due to fusion reactions in the core,  $S_{\text{D+T} \rightarrow \text{He}} \sim 1.75 \cdot 10^{20}/\text{s}$ . As a consequence of increased plasma dilution, a slight degradation in fusion performance from  $P_{\text{fus}} \sim 550$  MW to  $P_{\text{fus}} \sim 490$  MW can be observed, as the He concentration increases from  $\sim 2\%$  to  $\sim 4.5\%$ .  $Z_{\text{eff}} \sim 1.35$  in stationary conditions. Temperature screening in the edge region keeps the core Ne density at a comparably low level of  $n_{\text{Ne,core}} \sim 2.5\text{--}3.0 \cdot 10^{17}/\text{m}^3$ , corresponding to core fractional concentration  $\langle n_{\text{Ne}} \rangle / \langle n_e \rangle = \sim 0.25\%$ . Without the temperature screening effect, the core Ne density may be increased by  $\sim 10^{17}/\text{m}^3$  for the same Ne density at the separatrix. The total core radiation in stationary conditions amounts to  $P_{\text{rad,core}} \sim 25$  MW (consisting of  $\sim 8$  MW of impurity induced emission,  $\sim 14$  MW of bremsstrahlung due to interaction with main ions and  $\sim 3$  MW of synchrotron radiation). Other important core parameters in quasi-stationary conditions:  $Q_{\text{fus}} \sim 9.0\text{--}9.5$ ,  $H_{98,y} \sim 0.95$ ,  $\beta_N \sim 2.05\%$ ,  $P_{\text{sep}} \sim 135$  MW.

#### 4.2. Complete transition from high $Q_{\text{fus}}$ to late ramp-down

Continuing from the late stationary flat-top phase at  $Q_{\text{fus}} \sim 9\text{--}10$ , the current ramp-down phase has been simulated for the period until  $I_{\text{pl}} \sim 3$  MA during which the plasma can be expected to remain in diverted configuration. At the time of the start of current ramp-down, the He density in the core has already approached but not yet reached quasi-stationary conditions. The total He content can therefore increase slightly in the early ramp-down phase. Pellet fuelling has been completely switched off for the entire current ramp-down phase. To trigger the back transition to L-mode, auxiliary heating is completely switched off at a specified current level. The plasma then quickly transitions into ELM free H-mode, degraded type-III ELMy H-mode and finally returns back to L-mode. To avoid detachment, ECRH is applied again in the early L-mode phase at  $P_{\text{EC}} = 10\text{--}20$  MW. D+T and Ne puff rates are adjusted in order to maintain the divertor peak heat load below  $10 \text{ MW}/\text{m}^2$ , to keep the ion temperature below the critical level for W sputtering ( $T_i < \sim 5$  eV) in the region on the divertor plates with maximum ion current density, and to avoid plasma detachment. The nominal D+T gas puff rate is typically maintained at a level of  $\Gamma_{\text{DT,neut}} \sim 10^{22}/\text{s}$  and then

quickly reduced to a very low level before the H-L transition. The Ne puff rate is feedback controlled in the H-mode phase to maintain a prescribed target level for Ne radiation in the SOL and private region, and is gradually reduced to zero before the plasma returns back to L-mode. It is also possible in simulations to reduce the Ne content by artificially reducing the recycling. Given these modelling uncertainties, it is difficult to estimate from the simulations the level of pumping that will be required to remove Ne from the SOL and avoid detachment in the early L-mode phase. However, the simulations indicate that a safe H-L transition could in principle be achieved for a given targeted evolution in Ne induced radiation in the SOL and private region. The question of Ne pump efficiency in the transition phase are addressed Section 4.4 where dedicated recalculations of the H-L transitions without Ne puff feedback control are presented. Two ramp-down cases with different times for the H-L transition have been modelled:

- C1. Early H-L transition at  $I_{pl} \sim 15$  MA: Auxiliary heating is completely switched off at  $I_{pl} < 15$  MA while the plasma remains in H-mode. Zero edge loop voltage is prescribed for the entire current ramp-down phase.
- C2. Late H-L transition at  $I_{pl} \sim 10$  MA: Auxiliary heating is completely switched off at  $I_{pl} < 10$  MA while the plasma remains in H-mode. The edge loop voltage is reduced from 0 V down to -0.1 V in the late H-mode phase and further down to -0.3 V in the late L-mode phase to speed up the reduction in plasma current and to reduce resistive flux consumption.

The plasma evolution for ramp-down Cases C1 and C2 is shown in Figs. 17-23 (early H-L transition: blue, late H-L transition: red).

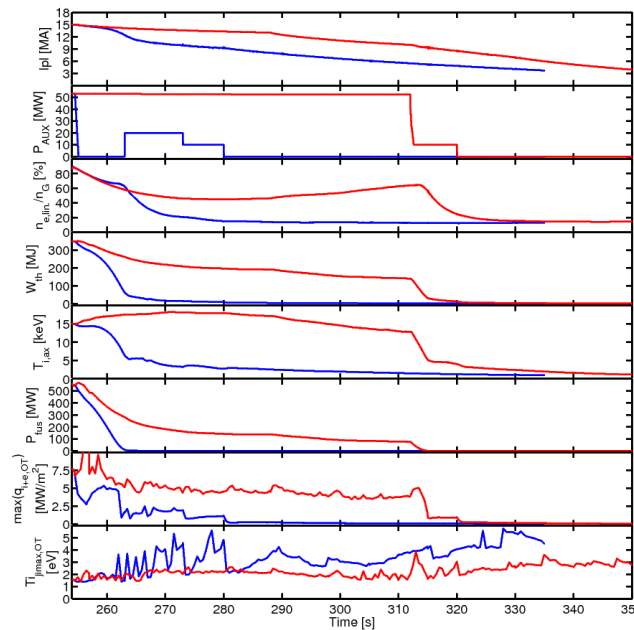


**Figure 17.** Time evolution of plasma current, auxiliary power, Greenwald density fraction, thermal energy content, ion temperature on axis, fusion power, the maximum power density at the outer target (considering power transferred by electrons, ions and due to recombination) and ion temperature at the outer target location with the maximum absolute value of ion current density (from top to bottom) during the current ramp-down for  $I_{pl} = 15 \rightarrow 3$  MA for an H-L transition at  $I_{pl} \sim 15$  MA (blue) and  $I_{pl} \sim 10$  MA (red).

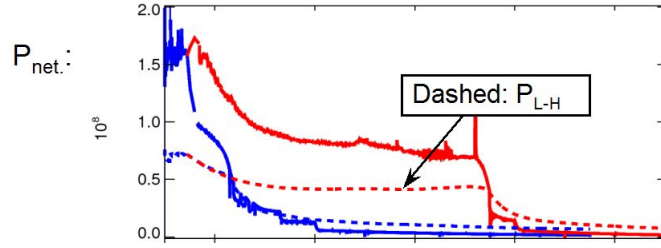


**Figure 18.** Time evolution of net power (solid) vs. L-H transition power threshold (dashed), during the current ramp-down for  $I_{pl} = 15 \rightarrow 3$  MA for an H-L transition at  $I_{pl} \sim 15$  MA (blue) and  $I_{pl} \sim 10$  MA (red).

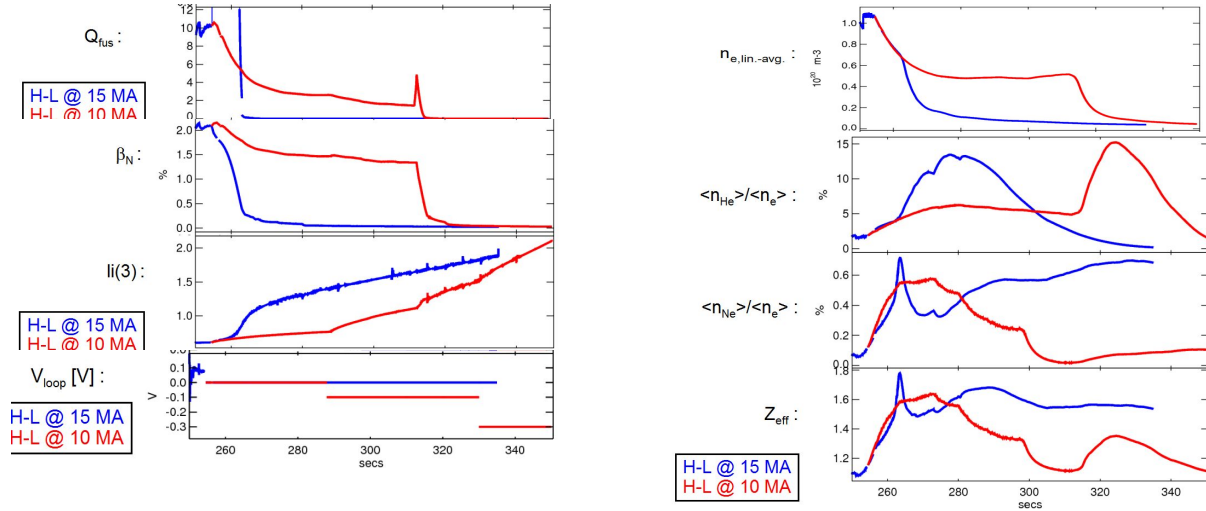


**Figure 19.** Left: Time evolution of fusion  $Q$ , normalised beta, internal inductance  $li(3)$  and loop voltage, right: time evolution of line-averaged electron density, He core concentration, Ne core concentration and  $Z_{eff}$  (from top to bottom), during the current ramp-down for  $I_{pl} = 15 \rightarrow 3$  MA for an H-L transition at  $I_{pl} \sim 15$  MA (blue) and  $I_{pl} \sim 10$  MA (red).

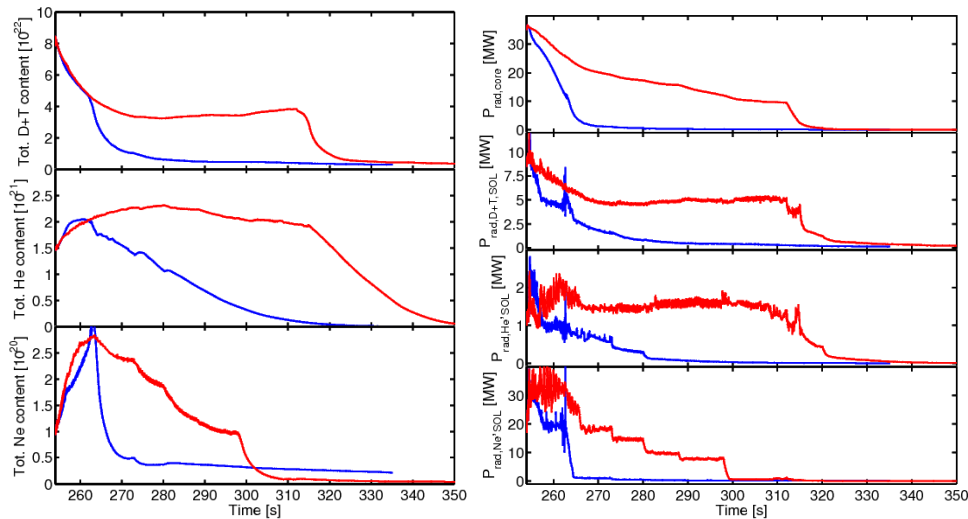


**Figure 20.** Left: Time evolution of total D+T (top), He (middle) and Ne (bottom) ion content in the core, SOL and private region, right: Time evolution of core radiation, D+T induced, He induced radiation and Ne induced radiation (from top to bottom) in the SOL and private region, during the current ramp-down for  $I_{pl} = 15 \rightarrow 3$  MA for an H-L transition at  $I_{pl} \sim 15$  MA (blue) and  $I_{pl} \sim 10$  MA (red).

Simulation results shown in Figs. 17-22 indicate that a ramp in current from high  $Q_{fus}$  H-mode at  $I_{pl} = 15$  MA to L-mode at  $I_{pl} = 3$  MA respecting PF coil current, fuelling, heating and divertor operational constraints can be achieved, and core impurity contamination can be kept at a moderate level. The internal inductance increases significantly towards the end of ramp-up which may become challenging for vertical stability control [de Vries NF 2017]. To

mitigate that increase, the continued application of  $P_{\text{AUX}}$  until late ramp-down and a gradual reduction in plasma elongation could be considered.

Fig. 17 shows that the density can be reduced quickly enough to avoid reaching the Greenwald density limit with zero pellet fuelling even for the earlier H-L transition with higher  $|dI_{\text{pl}}/dt|$  (cf. Fig. 17).

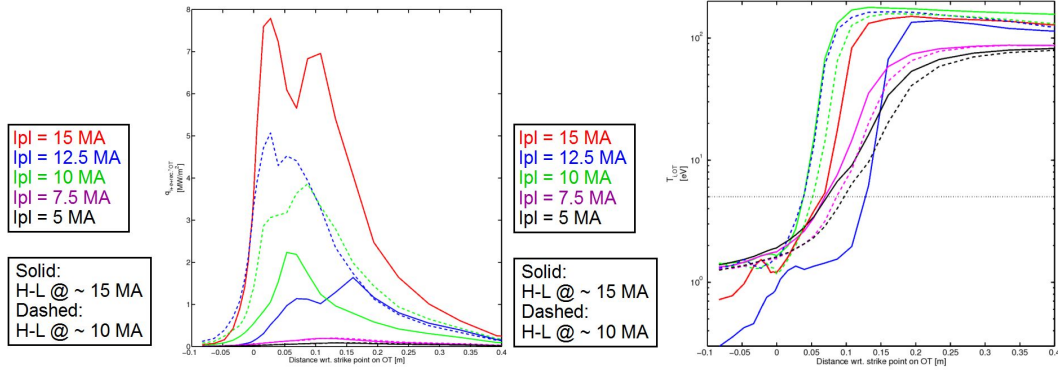


**Figure 21.** Profiles of power flux density (left) and ion temperature (right) at the outer target (including power from electrons, ions and recombination) at  $I_{\text{pl}} = 15$  MA (red), 12.5 MA (blue), 10 MA (green), 7.5 MA (magenta) and 5 MA (black) during the current ramp-down for an H-L transition at  $I_{\text{pl}} \sim 15$  MA (solid) and  $I_{\text{pl}} \sim 10$  MA (dashed).

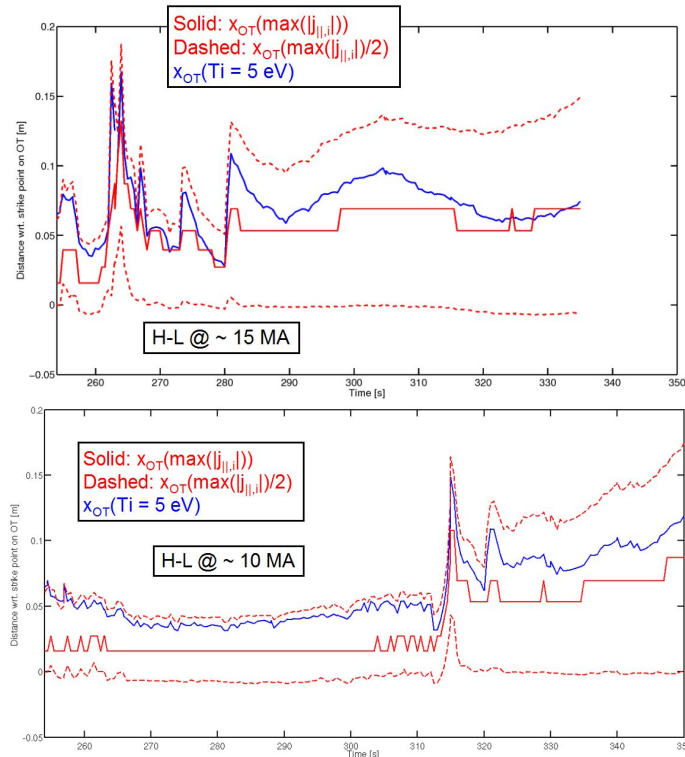


**Figure 22.** Time evolution of the locations on the outer divertor target where  $T_i \sim 5$  eV (blue colour, solid), where the maximum ion current density is reached (red colour, solid) and where half of the maximum ion current density is obtained (red colour, dashed) during the current ramp-down for the case of an H-L transition at  $I_{\text{pl}} \sim 15$  MA (Case C1, top) and at  $I_{\text{pl}} \sim 10$  MA (Case C2, bottom).

For divertor control, a late H-L transition at lower plasma current appears to be favourable despite reduced H-L transition times due to lower  $dW_{\text{th}}/dt$  and lower  $P_{\alpha}$ , as the heat flux to the divertor would already have approached a rather benign level and Ne could be completely pumped out from the plasma by the time  $I_{\text{pl}} \sim 10$  MA is reached if the plasma current is ramped down in H-mode at a constant negative edge loop voltage of less than a few hundred mV (cf. Figs. 18-20).

Slight differences in gas fuelling requirements for the Ohmically heated early current ramp-up vs. the late current ramp-down phase in L-mode ( $\sim 50\%$  increased  $\Gamma_{D+T,neut}$  for  $I_{pl} \sim 4\text{MA}$  at ramp-up) may be related to different current density shapes (hollow vs. strongly peaked) that seem to affect transport conditions due to different values for the safety factor, giving lower  $T_e$  in the core, lower resistivity and therefore a  $\sim 50\%$  increased  $P_{sep}$  driven by Ohmic heating at ramp-up. At high  $|dI_{pl}/dt|$  i.e. in case of a fast change in core particle content, divertor control by D+T gas puff adjustment might be slightly more challenging in the late ramp-down phase as compared to the early ramp-up phase. This is because the divertor density reacts more sensitively to a variation in D+T gas puff rates during current ramp-up when the puffed particles are partly transported to the confined region, increasing the core plasma density, while the total particle source in the SOL is to some extent controlled by the net particle efflux from the confined region in the ramp-down phase due to the reduction in core density.

In the late current ramp-down phase at densities below  $\sim 10^{19}/\text{m}^3$ , it may become difficult to simultaneously avoid detachment and maintain  $T_i < 5\text{ eV}$  in the vicinity of the strike points (cf. Figs. 21-22). However, W sputtering rates may be small even if the critical temperature threshold is exceeded as ion current densities have dropped to very low levels. Furthermore, W sputtering in the late current ramp-down phase might not be problematic for plasma operation.

#### 4.3. Current ramp-down in H-mode at zero loop voltage

Case C2 from Section 4.2 with late transition from H-mode to L-mode at  $I_{pl} \sim 10\text{ MA}$  has been rerun with a fixed loop voltage at the boundary of  $0\text{ V}$  (referenced as Case C3). The temperature remains high ( $T_{e,ax} \sim 15\text{-}20\text{ keV}$ ) while the  $P_{AUX}$  remains at  $53\text{ MW}$  and plasma stays in H-mode, while density rapidly falls to  $\sim 0.5 \cdot n_{GW}$  after pellet fuelling stops at the beginning of the  $I_{pl}$  ramp-down. Therefore, resistive flux losses are almost as small as in the flat-top phase. Consequently, the inductive flux and  $I_{pl}$  fall very slowly at zero loop voltage. It might therefore be possible to significantly extend the H-mode duration during current ramp-down in line with findings from studies for the ITER baseline scenario presented in [Parail NF 2013].

The plasma evolution for the simulation of current ramp-down in H-mode at  $U_{loop,sep} = 0\text{ V}$  is shown in Fig. 23 in magenta. For comparison, simulation results for Case C2 from the previous subsection are also displayed in red.

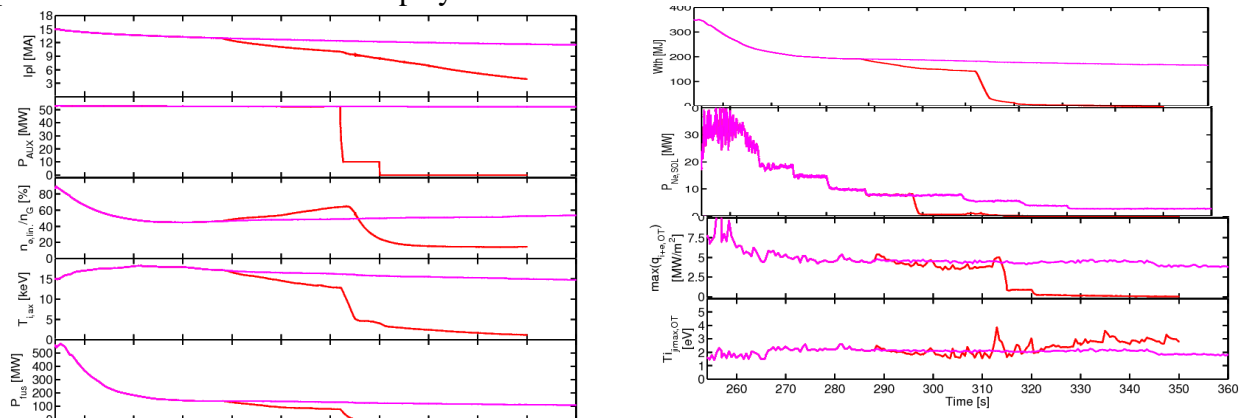


**Figure 23.** Left: Time evolution of plasma current, auxiliary power, Greenwald density fraction, ion temperature on axis and fusion power, right: time evolution of the thermal core energy content, Ne induced radiation in the SOL and private region, the maximum power flux density at the outer target and ion temperature at the outer target location with the maximum absolute value of ion current density (from top to bottom), during current ramp-down in H-mode for cases C3 (magenta) and C2 (red) discussed in the text.

Case C3 confirms that the neutron yield could be significantly enhanced by extension of the H-mode duration by up to a few hundred of seconds into the current ramp-down phase with zero boundary loop voltage application if the auxiliary heating is maintained but pellet fuelling is switched off at the beginning of current ramp-down. This is due to low resistive flux consumption ( $\sim 0.03$  Wb/s), yielding a slow reduction in inductive flux and thus  $I_{pl}$  at  $U_{loop,sep} = 0V$ . Ne seeding can be gradually reduced from the start of the ramp-down, but it is still needed while  $P_{AUX}$  remains at 53MW and  $I_{pl} \geq \sim 12-13$  MA.

As indicated in the baseline optimisation studies in [Parail NF 2013, Koechl EPS 2012],  $P_{fus}$  could be significantly enhanced by a slight increase in  $n_{e,lin.-avg.}/n_{GW}$  to  $\sim 65\%$  by continued pellet fuelling at reduced injection rate, and it may be possible to further extend the H-mode duration in the ramp-down phase by exploitation of reduced margins required for PF coil current control at lower currents as they scale with  $I_{pl}$ , permitting the application of a small positive  $U_{loop}$ . That way, the neutron yield could be increased by  $> \sim 50\%$  compared to the baseline scenario configuration without extended ramp-down duration in H-mode.

#### 4.4. Refined calculations of the H-L transition during current ramp-down

The simulations of the transition from stationary high quality H-mode to L-mode at  $I_{pl} \sim 15$  MA and  $I_{pl} \sim 10$  MA that were presented in Subsection 4.2 (Cases C1-2) have been repeated with improved accuracy to study possibilities for the control, by D+T puff and Ne seeding, of power loads and temperature on the divertor targets during the transition. These new runs, referenced as Cases D1 and D2 for the early and late H-L transition, respectively, have been carried out with increased precision in the calculation of SOL transport by application of adaptive partial coupling with a reduced maximum allowed proportion of the non-coupling and full coupling time intervals  $\Delta t_1/\Delta t_2 = 10$ , and ensuring correction fluxes for main ions and impurities in the SOL remain  $\leq \sim 1\%$  with respect to reference fluxes. This may be important to accurately model the transient evolution of the SOL plasma on shorter time scales as they may occur in the H-L transition phase, while the error due to partial coupling with normal accuracy as used for Cases C1-3 as presented in the previous subsections is insignificant for slow transients as they occur in all other phases during current ramp-down. In addition to this, main ion and Ne puff rates are manually prescribed and adjusted in Cases D1-2, i.e. no feedback control has been applied. The applied puff rates are changed in time to assure a safe transition avoiding detachment and excessive power loads on the target plates during and after the transition. The fuelling scheme was adapted in order to keep the ion temperature below  $\sim 5$  eV in regions where the ion current densities tend to peak. Handling the H-L transition at  $I_{pl} \sim 10$  MA should be less challenging due to a reduced initial energy content at the start of the transition phase and because Ne seeding can be very low (as alpha heating has already reduced to a marginal level and heat fluxes entering the SOL have become substantially lower). However, it might be difficult to avoid detachment immediately after the H-L transition at  $I_{pl} \sim 15$  MA due to a very slow reduction in the Ne particle content in the SOL that is caused by a strong continuous core efflux of Ne into the SOL saturating the pumping capability.

The plasma evolution for the improved calculation of the H-L transition is shown in Figs. 24-28 (early H-L transition: blue, late H-L transition: red).

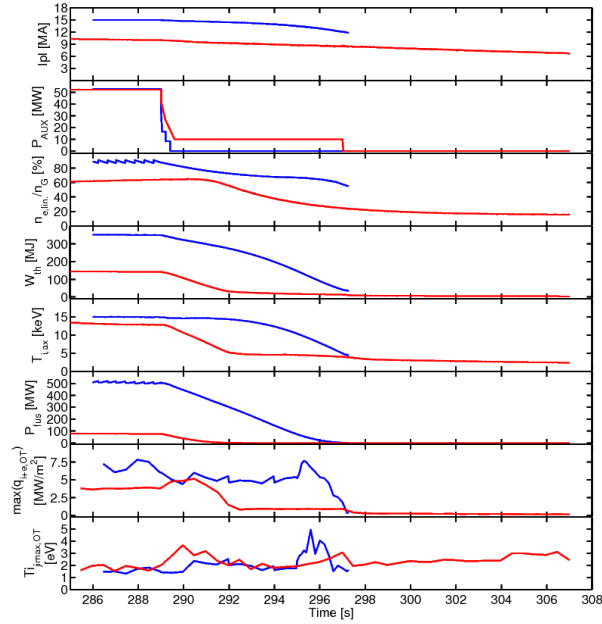


**Figure 24.** Time evolution of plasma current, auxiliary power, Greenwald density fraction, thermal core energy content, ion temperature on axis, fusion power, the maximum power density at the outer target (considering power transferred by electrons, ions and due to recombination) and ion temperature at the outer target location with the maximum absolute value of ion current density (from top to bottom) for the refined calculation of the H-L transition phase during current ramp-down occurring at  $I_{pl} \sim 15$  MA (blue) and  $I_{pl} \sim 10$  MA (red, shifted in time to match NB power switch off times).

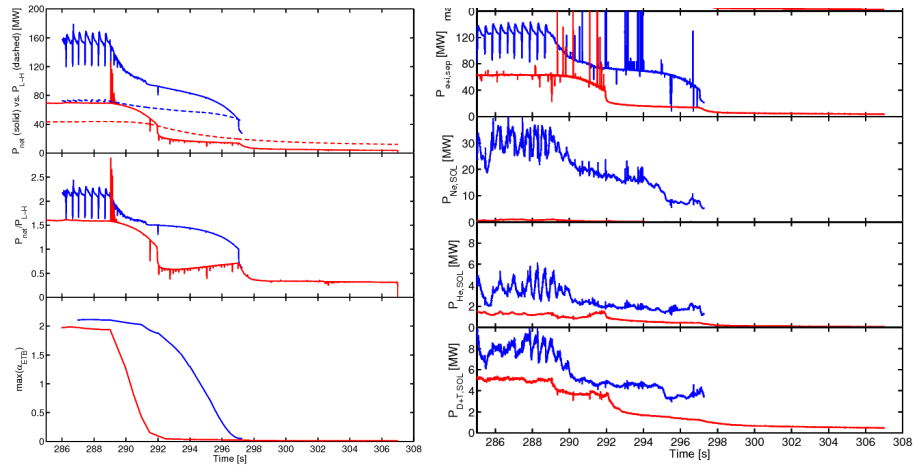


**Figure 25.** Left: Time evolution of the net power (solid) vs. the L-H transition power threshold (dashed), the ratio between the net power and the L-H transition power threshold and the maximum normalised pressure gradient in the ETB, right: time evolution of the thermal energy heat flux at the separatrix, the Ne, He and D+T induced radiation in the SOL and private region (from top to bottom), for the refined calculation of the H-L transition phase during current ramp-down occurring at  $I_{pl} \sim 15$  MA (blue) and  $I_{pl} \sim 10$  MA (red, shifted in time to match NB power switch off times).

Simulation results shown in Figs. 24-25 indicate that the duration of the transition from good quality H-mode to L-mode is long enough in order to ensure plasma shape and position control during the transition as described in [Loarte NF 2014, Parail NF 2013]. The duration is longer for the transition at high current ( $I_{pl} \sim 15$  MA:  $\sim 8$  s,  $I_{pl} \sim 10$  MA:  $\sim 3$  s), as the thermal energy content is considerably higher at the start of the transition, and because of alpha heating remaining significant during the transition.

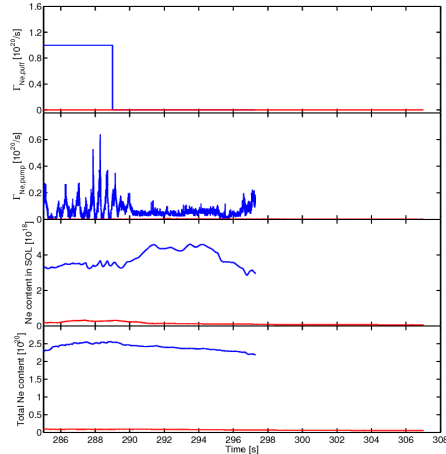


**Figure 26.** Time evolution of the Ne puff rate, the Ne pump rate, the Ne particle content in the SOL and the total Ne particle content in the core, SOL and private region (from top to bottom), for the refined calculation of the H-L transition phase during current ramp-down occurring at  $I_{pl} \sim 15$  MA (blue) and  $I_{pl} \sim 10$  MA (red, shifted in time to match NB power switch off times).

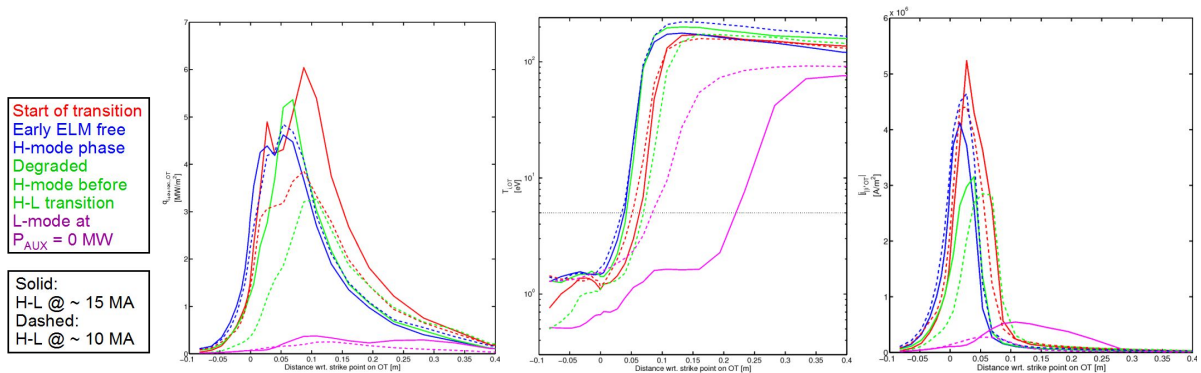


**Figure 27.** Profiles of power density (left), ion temperature (middle) and the absolute value of the ion current density (right) at the outer target, for the refined calculation of the H-L transition phase during current ramp-down occurring at  $I_{pl} \sim 15$  MA (solid) and  $I_{pl} \sim 10$  MA (dashed) at several stages during and after the duration phase (red: start of transition, blue: early ELM free H-mode phase, green: degraded H-mode before H-L transition, magenta: L-mode without auxiliary heat application). The heat flux is increased again at the time when the plasma is in a degraded H-mode regime for the H-L transition at  $I_{pl} \sim 15$  MA, as the DT gas puff rate has been reduced to a very low level just before the H-L transition in order to reduce the risk of detachment after the H-L transition due to Ne contamination.

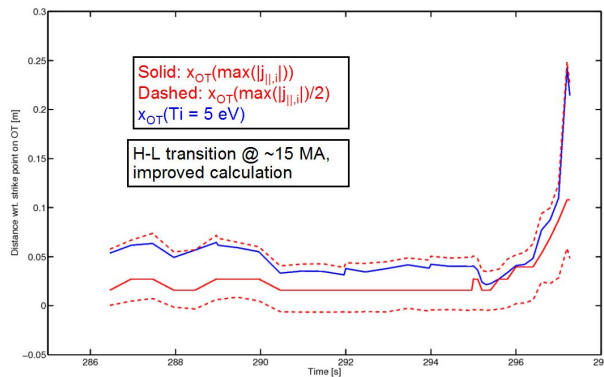


**Figure 28.** Time evolution of the locations on the outer divertor target where  $T_i = 5$  eV (blue colour, solid, lower  $T_i$  achieved at lower distance wrt. strike point location), where the maximum ion current density is reached (red colour, solid) and where half of the maximum ion current density is obtained (red colour, dashed) for the refined calculation of the H-L transition phase during current ramp-down occurring at  $I_{pl} \sim 15$  MA.

Figs. 22 and 27-28 show that the maximum heat flux on the divertor targets could be kept below  $10 \text{ MW/m}^2$  and the ion temperature in the vicinity of the strike points be maintained

below  $\sim 5$  eV by careful adjustment of DT gas fuelling and Ne seeding. However, it may become difficult to avoid detachment in the early L-mode phase after the H-L transition in the case that the DT puff rate is also reduced to negligible levels, as it seems that the Ne particle content in the SOL can only marginally be reduced during the transition even if Ne seeding is completely switched off at the start of the transition. Achieved Ne pump rates appear to be similar to the Ne flux from the core. In complementary simulations that are not shown here, it has been confirmed that the Ne pump efficiency can be slightly enhanced by application of higher DT gas puff rates, however, the range in applicable DT gas puff rates during the transition appears to be limited to a few  $10^{22}/s$  in the early phase of the transition and to only  $\sim 1.0-1.5 \cdot 10^{22}/s$  in the later phase.

At lower currents, Ne seeding requirements are much less severe. For  $I_{pl} < \sim 12-13$  MA, the Ne seeding rate can be zeroed as the Ne SOL content required for divertor protection is sustained by the Ne core efflux depleting the core on a time scale  $\tau_{\text{core Ne red.}} = \int n_{Ne} dV / \Gamma_{\text{pump, Ne}} \sim 40$  s. This large uncontrolled core efflux of Ne, combined with limited Ne pumping, will make it difficult to reduce SOL Ne radiation fast enough to avoid detachment in Case D1 (cf. Figs. 26-27), unless additional  $P_{AUX}$  is applied as done for the late H-L transition at 10 MA (Case D2). Determination of the minimum required auxiliary power to avoid detachment after an H-L transition at  $I_{pl} \sim 15$  MA would require further dedicated simulations with improved accuracy. If the plasma is ramped down in H-mode to  $I_{pl} \sim 10$  MA at  $U_{\text{loop, sep}} > \sim -0.1$  V, the Ne particle content in the core and SOL may be expected to already be negligible at the time of the H-L transition. For that reason, the problem with detachment in L-mode due to Ne contamination does not appear in the simulations of a late H-L transition.

## 5. Summary

This paper has presented coupled core+edge+SOL transport simulations (using JINTRAC) of the complete 15 MA 5.3 T DT ITER baseline scenario in the diverted phase, focussing on fuelling requirements for core density and divertor heat load control in non-stationary phases.

As the main key result from this study, the JINTRAC simulations have demonstrated that viable ITER plasma scenarios are conceivable, with the available fuelling actuators (pellets, gas puff and impurity seeding) and PF coil current and heating actuators, to robustly access the high  $Q_{fus}$  H-mode scenario required to demonstrate  $Q_{fus} = 10$  with  $P_{AUX} \leq 53$  MW. Furthermore, simulations suggest that a controlled back transition to L-mode and reduction in current to terminate the discharge is possible, respecting all main operational constraints throughout the entire scenario. The operational constraints can be summarised as follows:

- Constraints related to divertor control:
  - Maintenance of low ion temperatures  $< \sim 5$  eV near the strike point locations on both divertor targets for the avoidance of excessive W sputtering.
  - Maintenance of divertor heat loads below limit of  $\sim 10$  MW/m<sup>2</sup>.
  - Avoidance of complete divertor detachment.
- Core density control:
  - Maintenance of core density below or close to the Greenwald density limit.
  - Constraints on the density evolution after the L-H transition to ensure a robust access to a high density high  $Q_{fus}$  burning regime.
  - Upper limit in pedestal density to avoid core impurity accumulation via temperature screening in critical phases of the discharge.
- Constraints on  $P_{AUX}$ :
  - Maximum available auxiliary EC power of 20 MW and NB power of 53 MW.

- Satisfying the NB shine through limit ( $P_{\text{NB,shine-through}}/P_{\text{NB}} < \sim 10\%$  [Polevoi NF 2013]).
- Operational constraints imposed by PF coils and current control:
  - Upper limit in total poloidal flux consumption.
  - Maximum achievable current ramp rate.
  - Upper and lower limits on internal inductance  $li(3)$ .
  - Times for the variation in  $\beta_{\text{pol}}$  and  $li(3)$  during transients must exceed PF coil current feedback control times.
  - Lower limit in plasma current for full bore plasma divertor configuration.

The simulations notably include all challenging transient phases in the diverted phase. Our study is not exhaustive. Several additional constraints may be required in the experiment to control sawteeth and NTMs [Poli NF 2018], and to optimise ELM suppression/mitigation systems [Loarte NF 2014b]. In addition, this study has not fully taken into account the time delays for certain diagnostics (e.g. for the processing of raw measurement data) and actuators (e.g. response times of a few hundred milliseconds for the gas injection system [Bonnin NME 2017]) [Snipes NF 2017]. Some of these deficiencies are foreseen to be addressed in future work via IMAS workflow simulations in which JINTRAC may be directly coupled to the current design of the ITER Plasma Control System (PCS).

The full plasma scenario simulations reported in this paper confirm several findings from earlier modelling work relating to the optimisation of the core plasma, including: establishment of schemes for current ramp-up optimisation with respect to poloidal flux consumption and the safety factor at the start of flat-top [Parail NF 2009, Imbeaux NF 2011, Parail NF 2013]; limitation in achievable density for purely gas fuelled plasmas [Romanelli NF 2015]; compatibility with PF coil current shape and stability control constraints [Parail NF 2013]; challenges for density ramp after L-H transition to high  $Q_{\text{fus}}$  at low  $P_{\text{sep}}/P_{\text{L-H}}$  [Loarte NF 2013, Koechl NF 2017]; pellet fuelling requirements to achieve high density high  $Q_{\text{fus}}$  scenario [Garzotti NF 2012, Garzotti NF 2019]; challenge for divertor control due to pellet-induced perturbations [Wiesen NF 2017]; and H-L transition time exceeding feedback reaction time for plasma position control [Parail NF 2013, Loarte NF 2014].

The simulations presented here have also made a number of new findings. Firstly during the L-mode  $I_{\text{pl}}$  ramp-up:

- Operational range in  $n_{\text{e,lin.-avg.}}/n_{\text{GW}}$  is restricted to  $\sim 20 \pm 5\%$  for  $P_{\text{AUX}} \sim 10\text{-}20$  MW during ramp-up because of the simultaneous requirements: to keep  $T_i < \sim 5\text{eV}$  near strike points to minimise W sputtering; keeping SOL stable by keeping its density below the detachment threshold; and keeping power flux densities on the target plates below  $10 \text{ MW/m}^2$ .
- Pure Ohmic heating should be avoided during the  $I_{\text{pl}}$  ramp up because: high poloidal flux consumption would limit the maximum burn duration; with  $P_{\text{AUX}} = 0$  the achievable  $n_{\text{e,lin.-avg.}}/n_{\text{GW}}$  may be very low ( $\leq \sim 15\%$ ); and divertor control could be difficult when there is a sudden increase in  $P_{\text{AUX}}$  from  $P_{\text{AUX}} = 0$ .

Secondly, transition to high quality  $Q_{\text{fus}}$  H-mode may be more difficult if the L-H transition is at low  $I_{\text{pl}}$  for the following reasons:

- If the  $I_{\text{pl}}$  ramp-up continues in H-mode, the current induced at the edge takes longer to diffuse to the core, and  $li(3)$  is likely to drop below the critical value for shape control [Mattei FED 2009]. Reducing the  $I_{\text{pl}}$  ramp-up rate to keep an acceptable  $li(3)$  would significantly reduce the maximum burn duration. Furthermore plasma transport may be significantly degraded during the  $I_{\text{pl}}$  ramp-up, while  $s/q$  is reduced in the core [Parail 2013].

- The achievable  $W_{th}$  in stationary H-mode is significantly reduced after a transition at lower  $I_{pl}$  (e.g. 10 MA), the core  $T_i$  may not significantly exceed 10 keV (the critical temperature for the onset of fusion reactions and alpha heating), and it becomes more difficult to keep  $P_{net} \gg P_{L-H}$ . This extends the post-transition phase where divertor control may be challenging, delays the post L-H density ramp, and reduces the maximum burn duration.
- Pellet injection may be required after an early NB triggered L-H transition to keep density above the NB shine-through limit, further complicating the transition to a high quality H-mode. The plasma would stay closer to the L-H threshold, which increases the risk of failure to reach high  $Q_{fus}$ . In addition, the divertor may need to be operated closer to the density limit for full detachment after the L-H transition. Due to increased divertor control challenges after an early L-H transition, small-size pellets need to be injected to reduce transient edge plasma perturbations triggered by pellets. As the pellet fuelling efficiency is reduced at lower plasma edge temperatures, the fuelling throughput due to core fuelling may be significantly enhanced in this phase.

Thirdly, in the case of an L-H transition after the end of the  $I_{pl}$  ramp-up, the transition to high quality high  $Q_{fus}$  H-mode is predicted to be easier to achieve, however, as described in [Loarte NF 2013, Koechl NF 2017], the core density needs to be increased slowly and cautiously to ensure that the power near the separatrix stays well above  $P_{L-H}$ . Ne seeding might not be required while the pedestal pressure has not yet approached the edge MHD limit, as the power density at the targets can be maintained below  $10 \text{ MW/m}^2$  by adjustment of D+T puff rates only. However, as soon as the pedestal pressure and the core energy content have approached the limit imposed by edge MHD and core transport stiffness constraints, the heat flux to the SOL is predicted to increase on the energy confinement time scale. To accommodate this increase, significant Ne needs to be present in the SOL at this time. The exact start time of the ELMy H-mode phase needs to be anticipated in order to trigger the Ne seeding at the right time to provide the required level of SOL radiation. This critical phase of the scenario for the control of impurity radiation in the divertor may warrant further dedicated follow-up studies.

Finally, in the termination phase an H-L transition well into the  $I_{pl}$  ramp-down might be favourable from the point of view of divertor control. At lower  $P_\alpha$  and  $dW_{th}/dt$ , the divertor power flux will have approached a benign level, and Ne could have been almost completely pumped out of the plasma before the H-L transition. If Ne still needs to be present at the time of the H-L transition, the control of the SOL Ne concentration may be challenging, as Ne would need to be removed on short time scales that may not be possible with the limited available pumping and a significant Ne influx from the confined region. For an H-L transition at high current, auxiliary heating in the order of  $\sim 10\text{-}20 \text{ MW}$  may need to be applied at the start of the L-mode phase to avoid complete plasma detachment triggered by the remnant Ne population in the SOL causing substantial cooling at lower temperatures.

As a concluding remark, it is worth noting that some of the quantitative findings of the studies presented in this paper may be sensitive to detailed modelling assumptions that will need to be refined in the future as progress is made in the understanding of the physics processes that dominate plasma transport in the core, edge transport barrier, SOL and divertor.

### Acknowledgements

This work was funded jointly by the RCUK Energy Programme [grant number EP/I501045] and ITER Task Agreement C19TD51FE (implemented by Fusion for Energy under Grant GRT-502). The views and opinions expressed do not necessarily reflect those of Fusion for Energy which is not liable for any use that may be made of the information

contained herein. ITER is the Nuclear Facility INB no. 174. The views and opinions expressed herein do not necessarily reflect those of the ITER Organization.

## References

- [Albanese NF 2004] R. Albanese, M. Mattei and F. Villone 2004 Nucl. Fusion 44 999
- [Baylor SOFE 2015] L. Baylor et al., Proc. IEEE 26th Symposium on Fusion Engineering (Austin, USA, 31 May - 4 June 2015) SO18-3  
(<https://ieeexplore.ieee.org/stamp/stamp.jsp?tp=&arnumber=7482362>)
- [Belo EPS 2015] P. Belo et al., Proc. 42nd EPS Conf. on Plasma Physics vol 39E (Lisbon, Portugal, 22-26 June 2015) P4.120 (<http://ocs.ciemat.es/EPS2015PAP/pdf/P4.120.pdf>)
- [Bizarro PPCF 2016] J. P. S. Bizarro et al. 2016 Plasma Phys. Control. Fusion 58 105010
- [Bonnin NME 2017] X. Bonnin et al. 2017 Nucl. Mater. & Energy 12 1100
- [Braginski RevPP 1965] V. I. Braginski 1965 Review of Plasma Physics ed M. A. Leontovich (New York: Consultants Bureau)
- [Cenacchi JET-IR 1988] G. Cenacchi and A. Taroni 1988, "JETTO: A free-boundary plasma transport code (basic version)", JET Report JET-IR(88)03 JET Joint Undertaking
- [Challis NF 1989] C. D. Challis et al. 1989 Nucl. Fusion 29 563
- [Chang NF 2013] C. S. Chang et al. 2017 Nucl. Fusion 57 116023
- [Citrin NF 2012] J. Citrin et al. 2012 Plasma Phys. Control. Fusion 54 065008
- [de Vries NF 2017] P. C. de Vries et al. 2017 Nucl. Fusion 58 026019
- [Dux PPCF 2014] R. Dux et al. 2014 Plasma Phys. Control. Fusion 56 124003
- [Eich NF 2013] T. Eich et al. (2013) Nucl. Fusion 53 093031
- [Erba JET-R 1996] M. Erba et al. 1996, "Validation of a new mixed Bohm/gyro-bohm transport model on discharges of the ITER Data-base", JET Report JET-R(96)07 (<http://euro-fusionsci.org/archives/jet-archive/validation-of-a-new-mixed-bohmgyro-bohmtransport-model-on-discharges-of-the-iter-data-base>)
- [Erba PPCF 1997] M. Erba et al. 1997 Plasma Phys. Control. Fusion 39 261–276
- [Farina FsciTec 2007] D. Farina 2007 Fusion Sci. Technol. 52 154
- [Fichtmüller CJP 1998] M. Fichtmüller et al. 1998 Czech. J. Phys. 48/S2 25-38
- [Garzotti EPS 2016] L. Garzotti et al., Proc. 43rd EPS Conf. on Plasma Physics vol 40A (Leuven, Belgium, 4-8 July 2016) O4.113  
(<http://ocs.ciemat.es/EPS2016PAP/pdf/O4.113.pdf>)
- [Garzotti NF 2012] L. Garzotti et al 2012 Nucl. Fusion 52 013002
- [Garzotti NF 2019] L. Garzotti et al 2019 Nucl. Fusion 59 026006
- [Heikkinen PoP 1995] J.A. Heikkinen et al. 1995 Phys. Plasmas 2 3724
- [Hirvijoki CPC 2014] E. Hirvijoki et al. 2014 Comp. Phys. Comm. 185 1310-1321
- [Hogeweyj NF 2013] G.M.D. Hogeweyj et al. 2013 Nucl. Fusion 53 013008
- [Houlberg PoP 1997] W. A. Houlberg et al. 1997 Phys. Plasmas 4 3230
- [Imbeaux NF 2011] F. Imbeaux et al. 2011 Nucl. Fusion 51 083026
- [Kessel NF 2015] C. E. Kessel et al. 2015 Nucl. Fusion 55 063038 (12pp)
- [Kim NF 2018] S. H. Kim et al. 2018 Nucl. Fusion 58 056013 (17pp)
- [Koechl EPS 2012] F. Koechl et al., Proc. 39th EPS Conf. on Plasma Physics vol 36F (Stockholm, Sweden, 2-6 July 2012) P1.042  
(<http://ocs.ciemat.es/EPSICPP2012PAP/pdf/P1.042.pdf>)
- [Koechl NF 2017] F. Koechl et al. 2017 Nucl. Fusion 57 086023 (32pp)
- [Koechl PPCF 2018] F. Koechl et al. 2018 Plasma Phys. Control. Fusion 60 074008
- [Kukushkin PPCF 2002] A. S. Kukushkin and H.D. Pacher, Plasma Phys. Control. Fusion 44 (2002) 931–943
- [Kukushkin JNM 2013] A. S. Kukushkin et al. 2013 J. Nucl. Mater. 438 S203
- [Lauro-Taroni EPS 1994] L. Lauro-Taroni et al., Proc. 21st EPS Conf. on Controlled Fusion Plasma Physics vol 18B (Montpellier, France, 27 June-1 July 1994) p 102  
(<http://euro-fusionsci.org/archives/jet-archive/impurity-transport-of-high-performancedischarges-in-jet>)
- [Lipschultz NF 1984] B. Lipschultz et al. 1984 Nucl. Fusion 24 977
- [Loarte NF 2013] A. Loarte et al. 2013 Nucl. Fusion 53 083031
- [Loarte NF 2014] A. Loarte et al. 2014 Nucl. Fusion 54 123014
- [Loarte NF 2014b] A. Loarte et al. 2014 Nucl. Fusion 54 033007
- [Martin JPC 2008] Y.R. Martin et al 2008 J. Phys.: Conf. Ser. 123 012033
- [Mattei FED 2009] M. Mattei et al. 2009 Fusion Engineering and Design 84 300–304

- [Militello-Asp NF 2019] E. Militello-Asp et al., submitted to Nucl. Fusion  
[Pacher JNM 2015] H. D. Pacher et al. 2015 Journal of Nuclear Materials 463 591–595  
[Parail NF 2009] V. Parail et al 2009 Nucl. Fusion 49 075030  
[Parail NF 2013] V. Parail et al. 2013 Nucl. Fusion 53 113002  
[Pégourié NF 2005] B. Pégourié et al. 2005 Plasma Phys. Control. Fusion 47 17–35  
[Pégourié NF 2007] B. Pégourié et al. 2007 Nucl. Fusion 47 44–56  
[Polevoi NF 2013] A. R. Polevoi et al. 2013 Nucl. Fusion 53 123026  
[Polevoi NF 2015] A. R. Polevoi et al. 2015 Nucl. Fusion 55 063019  
[Poli FEC 2018] F. Poli et al., Proc. 27th IAEA FEC, Ahmedabad, India, 2018, paper EX/P7-27 (<https://nucleus.iaea.org/sites/fusionportal/Shared%20Documents/FEC%202018/fec2018-preprints/preprint0295.pdf>)  
[Poli NF 2018] F. M. Poli et al. 2018 Nucl. Fusion 58 016007  
[Reiter JNM 1992] D. Reiter 1992 J. Nucl. Mater. 196-198 80–9  
[Romanelli PFR 2014] M. Romanelli et al. 2014 Plasma and Fusion Research 9 3403023  
[Romanelli NF 2015] M. Romanelli et al. 2015 Nucl. Fusion 55 093008  
[Sartori PPCF 2004] R. Sartori 2004 Plasma Phys. Control. Fusion 46 723  
[Simonini CPP 1994] R. Simonini et al. 1994 Contrib. Plasma Phys. 34 368  
[Snipes NF 2017] J.A. Snipes et al. 2017 Nucl. Fusion 57 125001  
[Snyder PoP 2009] P. Snyder et al. 2009 Phys. Plasmas 16 056118  
[Summers ADAS 2001] H. P. Summers 2001 The ADAS manual version 2.3 (<http://adas.ac.uk>)  
[Summers AIP 2007] H. P. Summers et al. 2007 AIP Conf. Proc. 901 239  
[Waltz PoP 1997] R. E. Waltz et al. 1997 Phys. Plasmas 4 2482  
[Wiesen PPCF 2011] S. Wiesen et al 2011 Plasma Phys. Control. Fusion 53 124039  
[Wiesen NF 2017] S. Wiesen et al. 2017 Nucl. Fusion 57 076020